Cell

KDM4A Lysine Demethylase Induces Site-Specific Copy Gain and Rereplication of Regions Amplified in Tumors

Joshua C. Black,[1,8] Amity L. Manning,[1,8] Capucine Van Rechem,[1,8] Jaegil Kim,[3,8] Brendon Ladd,[1] Juok Cho,[3] Cristiana M. Pineda,[1] Nancy Murphy,[4] Danette L. Daniels,[4] Cristina Montagna,[5] Peter W. Lewis,[6] Kimberly Glass,[7] C. David Allis,[6] Nicholas J. Dyson,[1] Gad Getz,[2,3,*] and Johnathan R. Whetstine[1,*]

[1]Massachusetts General Hospital Cancer Center and Department of Medicine
[2]Massachusetts General Hospital Cancer Center and Pathology Department
Harvard Medical School, 13th Street, Charlestown, MA 02129, USA
[3]Broad Institute of MIT and Harvard, Cambridge, MA 02142, USA
[4]Promega Corporation, 2800 Woods Hollow Road, Madison, WI 53711, USA
[5]Department of Genetics, Pathology, Albert Einstein College of Medicine, Yeshiva University, Bronx, NY 10461, USA
[6]Laboratory of Chromatin Biology and Epigenetics, The Rockefeller University, New York, NY 10065, USA
[7]Department of Biostatistics and Computational Biology, Dana Farber Cancer Institute and Harvard School of Public Health, Boston, MA 02115, USA
[8]These authors contributed equally to this work
*Correspondence: gadgetz@broadinstitute.org (G.G.), jwhetstine@hms.harvard.edu (J.R.W.)
http://dx.doi.org/10.1016/j.cell.2013.06.051

SUMMARY

Acquired chromosomal instability and copy number alterations are hallmarks of cancer. Enzymes capable of promoting site-specific copy number changes have yet to be identified. Here, we demonstrate that H3K9/36me3 lysine demethylase KDM4A/JMJD2A overexpression leads to localized copy gain of 1q12, 1q21, and Xq13.1 without global chromosome instability. KDM4A-amplified tumors have increased copy gains for these same regions. 1q12h copy gain occurs within a single cell cycle, requires S phase, and is not stable but is regenerated each cell division. Sites with increased copy number are rereplicated and have increased KDM4A, MCM, and DNA polymerase occupancy. Suv39h1/KMT1A or HP1γ overexpression suppresses the copy gain, whereas H3K9/K36 methylation interference promotes gain. Our results demonstrate that overexpression of a chromatin modifier results in site-specific copy gains. This begins to establish how copy number changes could originate during tumorigenesis and demonstrates that transient overexpression of specific chromatin modulators could promote these events.

INTRODUCTION

Genomic instability is a major contributing factor to the development and onset of age-related diseases such as cancer (Maslov and Vijg, 2009; Negrini et al., 2010). Cancer cells are often characterized by copy number alterations: gains or losses of chromosome arms and/or whole chromosomes as well as amplifications of smaller genomic fragments (Beroukhim et al., 2010; Hook et al., 2007; Stratton et al., 2009). Genome-wide analysis of copy number changes in cancer has identified chromosomal regions with higher frequencies of amplification, which often contain putative oncogenes (Beroukhim et al., 2010). In some cases, the oncogenes have been shown to impact cellular behavior (e.g., *MYC* and *MCL1*), whereas other genes within these regions do not have clear connections with tumorigenesis. The lack of obvious connection does not preclude the gene's involvement. For example, cellular stresses can select for gene amplification that will promote cancer cell survival, as exemplified by the amplification of dihydrofolate reductase when cells are treated with methotrexate (Schimke, 1984). Even though cancer genomes frequently have altered chromosomal regions, there is little knowledge about the regulatory mechanisms or factors that are involved in promoting copy number alterations at specific regions of the genome.

Several mechanisms have been proposed for generating copy number variation (CNV). For example, many models for DNA amplification incorporate stalled replication forks and DNA double-strand breaks that are generated during replication. It has been proposed that these stalled/collapsed replication forks are associated with and can cause tandem duplications. A second mechanism proposed to contribute to CNV involves the use of breaks or repair intermediates as primers for rereplication of specific stretches of DNA, which can reincorporate into the genome, resulting in gene duplications or deletions. Alternatively, it is also possible that these events will not integrate in the genome (Hastings et al., 2009). A third mechanism that could generate rereplicated fragments and copy number alteration is the head-to-tail collision of elongating DNA polymerases (Davidson et al., 2006; Hook et al., 2007). Because chromatin structure impacts replication initiation and elongation efficiency as well as

DNA damage response and repair (Alabert and Groth, 2012; Papamichos-Chronakis and Peterson, 2013), the chromatin state or modifying enzyme(s) could have a significant impact on each of these possible mechanisms.

Recently, Kiang and colleagues demonstrated that local DNA fragment amplification occurs during S phase (Kiang et al., 2010) and that the chromatin context or chromosome microenvironments play a major role in this process. Consistent with an important role for the chromatin context, misregulation of the histone 4 lysine 20 monomethyltransferase KMT5A (H4K20me1, PR-Set7/Set8) promotes rereplication, at least in part, by increasing H4K20me2/3 levels and promoting ORC recruitment through binding of H4K20me2 (Beck et al., 2012; Kuo et al., 2012; Tardat et al., 2010). However, the role of methylation in modulating replication is not limited to the direct recruitment of DNA replication factors. For example, we have previously demonstrated that the H3K9me3 demethylase KDM4A/JMJD2A was able to increase accessibility and alter the replication timing at specific heterochromatic regions (Black et al., 2010). The regulation of KDM4A protein levels is also important in modulating its chromatin occupancy, replication initiation, and S-phase progression (Van Rechem et al., 2011). Furthermore, Mallette and colleagues demonstrate that increased KDM4A expression abrogates 53BP1 recruitment to DNA damage sites, suggesting a role for KDM4A in DNA damage response (Mallette et al., 2012). Therefore, we hypothesize that overexpression of catalytically active KDM4A may provide a potential enzymatic link to the proposed methods for generating copy number alterations through replication abnormalities, which may contribute to copy number changes in cancer.

In this study, we analyzed The Cancer Genome Atlas (TCGA) data and observed that *KDM4A* is amplified and overexpressed in several tumor types. KDM4A overexpression in transgenic cells was sufficient to promote copy gain of specific chromosomal domains (e.g., 1q12). KDM4A-dependent copy gain was induced in less than 24 hr and required S phase. These copy gains were not stably inherited but were generated transiently in each subsequent S phase and cleared by late G2. KDM4A was the only KDM4 family member that generated the gains in a catalytically dependent manner. These copy gains were antagonized by coexpression of Suv39h1/KMT1A or HP1γ, and H3K9 or H3K36 methylation interference promoted gain. Furthermore, KDM4A associated with replication machinery and promoted rereplication of regions exhibiting copy gain. KDM4A overexpression increased KDM4A, MCM, and DNA polymerase association as well as decreased HP1γ occupancy at regions that undergo KDM4A-dependent rereplication. Interestingly, focal amplifications of 1q21 and Xq13.1 were correlated with *KDM4A* amplification in tumors, which was recapitulated in KDM4A-overexpressing cell lines. Our findings demonstrate that KDM4A overexpression results in site-specific copy gain of regions amplified in human tumors.

RESULTS

KDM4A Is Amplified and Overexpressed in Cancer

KDM4A has previously been demonstrated to be overexpressed in breast and lung cancer (Berry et al., 2012; Mallette and Richard, 2012). However, a comprehensive profile of primary tumors for alterations in KDM4A expression levels has yet to be established. There are few insights into the mechanisms that promote increased expression in tumors. Therefore, we conducted a comprehensive analysis of *KDM4A* copy number and expression level in 1,770 primary tumor samples from eight different cancer types (Figure S1 available online) represented in TCGA (Beroukhim et al., 2010). We found evidence of increased *KDM4A* copy number (GISTIC annotation of +1 or +2; Mermel et al., 2011) in 18.9% of tumors (335 out of 1,770 samples; Figure 1A) and copy loss in 22.1% of tumors (392 out of 1,770 samples; Figure 1A). Furthermore, amplification or deletion of *KDM4A* resulted in increased or decreased *KDM4A* expression, respectively (Figures 1B and Figure S1A). *KDM4A* was both amplified and deleted across many disparate cancer types, and *KDM4A* expression correlated with copy number in these samples (Figures S1E–S1L). We also observed amplification and deletion of *KDM4B-D* in cancer, which correlated with expression (Figures S1B–S1D). These data provide a molecular basis for the elevated KDM4A levels observed in different tumor samples.

Ovarian cancer was significantly enriched for *KDM4A* amplification, which was amplified in 46% of the tumors (94 out of 204, $p = 1.4 \times 10^{-21}$ for gain versus no change and loss by Fisher's exact test), with relatively few examples of deletion (9.8%; 20 out of 204, samples) (Figures 1C and S1I). The amplification of *KDM4A* in ovarian cancer also correlated with increased expression (Figures 1D and S1I). In addition, *KDM4A* focal amplification (GISTIC +2) was significantly associated with the time to death in the ovarian cancer patient data set, with a median time to death of 691 days compared to 1,052 days without *KDM4A* amplification (Figure 1E, $p = 0.02$); however, *KDM4A* loss (GISTIC -2 or -1) was not significantly different from patients without changes in *KDM4A* copy number ($p = 0.85$). In sharp contrast to *KDM4A*, few cases of focal amplifications were observed for *KDM4B-D*, and no statistical significance was associated with their focal amplifications and time to death (Figures 1F–1H). However, focal deletion of *KDM4C* (GISTIC -2) and broad loss or gain (GISTIC -1 or +1) of *KDM4D* modestly associated with poor outcome ($p = 0.014$, $p = 0.013$, and $p = 0.018$, respectively). These data highlight the differences between the KDM4 family and cancer outcome, which suggests nonoverlapping functions in certain cancer types. These data also suggest that KDM4A levels could function as a biomarker in ovarian cancer.

KDM4A Overexpression Promotes Copy Gain of 1q12

We previously demonstrated that KDM4A overexpression promoted faster S-phase progression, increased chromatin accessibility, and altered replication timing (Black et al., 2010). KDM4A was also shown to impact the DNA damage response (Mallette et al., 2012). For these reasons, we hypothesized that KDM4A overexpression may promote genomic instability, which is a hallmark of cancer (Luo et al., 2009; Hanahan and Weinberg, 2011). Therefore, we stably overexpressed KDM4A in the karyotypically stable and immortalized, but not transformed, RPE1-hTERT (RPE) cell line (GFP, referred to as control or CTRL; GFP-KDM4A, referred to as KDM4A) (Jiang et al., 1999). Similar to our previously reported 293T stable cells (Figure S2A), RPE stable cell lines expressed KDM4A about 2- to 3-fold over

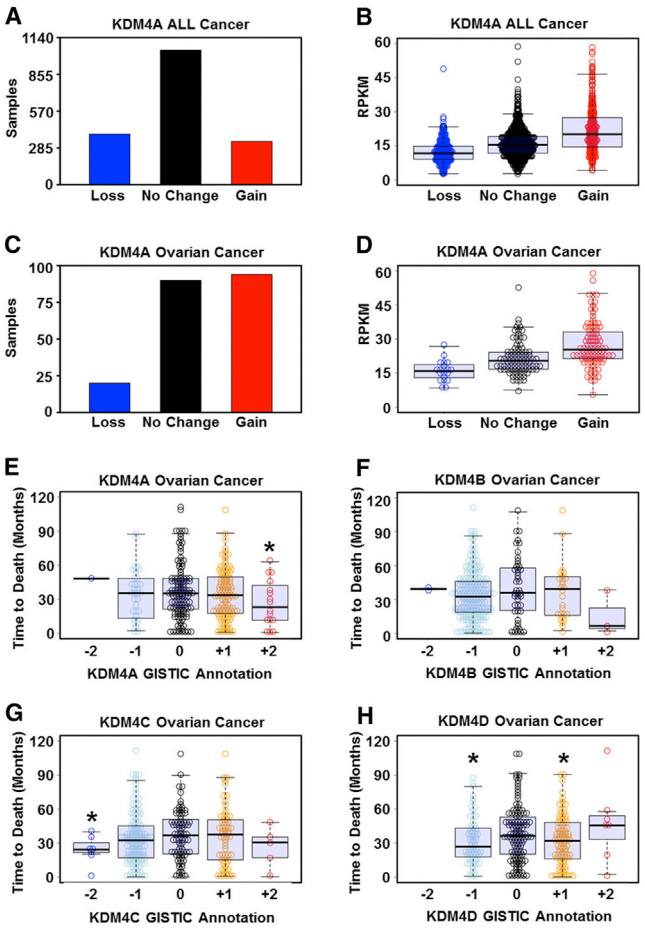

Figure 1. KDM4A Is Amplified and Overexpressed in Cancer and Correlates with Poor Outcome in Ovarian Cancer

(A) Distribution of gain (GISTIC annotation +1 or +2) or loss (GISTIC annotation −1 or −2) of copy of *KDM4A* in 1,770 cancer samples.

(B) Amplification of *KDM4A* correlates with increased expression of KDM4A in TCGA.

(C) *KDM4A* is frequently amplified in ovarian cancer ($p = 1.4 \times 10^{-21}$ for gain versus no change and loss by Fisher's exact test).

(D) Amplification of *KDM4A* in ovarian cancer correlates with increased expression of *KDM4A*.

(E) Focal amplification of *KDM4A* in ovarian cancer correlates with poor outcome in 285 deceased ovarian cancer samples ($p = 0.02$ by one-tailed Student's t test and 0.048 by one-tailed, Wilcoxon rank sum test for +2 versus 0).

(F) Copy number of *KDM4B* does not correlate with outcome in ovarian cancer.

(G) Deletion of *KDM4C* in ovarian cancer correlates with outcome ($p = 0.014$ for loss versus none).

(H) Copy number loss and gain of *KDM4D* correlate with outcome in ovarian cancer ($p = 0.018$ for gain versus none and 0.013 for loss versus none by Student's t test).

Asterisk indicates significant difference from no change samples ($p < 0.05$). RPKM denotes reads per kilobase exon model per million reads of RNA-seq data (see the Extended Experimental Procedures). See also Figure S1.

endogenous level (Figure S2B). Upon spectral karyotyping these cell lines, we did not observe major genomic events that were specific to the KDM4A cell lines when compared to CTRL cell lines (SKY; Figures 2A and 2B and Table S1). Similarly, G-band analysis of a 293T KDM4A-overexpressing stable cell line did not document any amplification, deletion, or translocation specific to GFP-KDM4A cells (data not shown). These data support the notion that modest KDM4A overexpression does not promote large-scale genomic instability.

We reasoned that KDM4A might promote instability at specific genomic loci that could be below the detection threshold of SKY. In order to identify these candidate regions, we reanalyzed our chromatin immunoprecipitation (ChIP) on chip analysis of KDM4A binding in 293T cells (Figure S2C) (Van Rechem et al., 2011) for KDM4A enrichment by cytogenetic band. Of the top ten enriched cytogenetic bands, only 1q12 was specifically enriched in KDM4A-overexpressing cells when compared to control cells (Figure S2C). 1q12/21 is a region with frequent CNV in lung cancer, multiple myeloma, and congenital heart abnormalities and has been described as a susceptibility locus for schizophrenia and autism (Brunet et al., 2009; Brzustowicz et al., 2000; Inoue et al., 2004; Yakut et al., 2006). To determine whether the copy number of 1q12 was altered following manipulation of KDM4A protein levels, we performed fluorescent in situ hybridization (FISH) in CTRL and KDM4A-overexpressing 293T cells (Figures 2C–2K and S2D). KDM4A overexpression resulted in increased copy number of 1q12h in 14% of cells (Figure 2K), which was not due to a gain of the entire 1q chromosome arm, as the 1q telomere did not have an increase in copy number (Figure 2K; 1qTel). Furthermore, no other gains occurred at additional pericentric regions (Figure 2K). We further validated these results in the RPE stable cell lines used in the SKY analysis (Figures 2A, 2B, S2B). Similar to the 293T cells, 17% of KDM4A-overexpressing RPE cells showed an increase in copy of 1q12h, whereas no significant changes in copy number were observed for the 1q telomere or other centromeres on chromosomes 2, 6, 8, or X (Figures 2L–2T; Chr 2, 6, 8, X).

To eliminate the possibility that KDM4A promoted chromatin accessibility so that there was increased 1q12h detection, condensin 1 (CapD2) or condensin 2 (CapD3) were depleted from cells (Figure S2F). Depletion of either condensin did not increase detection of 1q12h amplification in CTRL or KDM4A cells (Figure S2G). Therefore, the increased copy number of 1q12h in KDM4A cells is most likely not an artifact of increased chromatin accessibility. Furthermore, 1q12h copy gain was not due to alterations in p53 activity, as doxorubicin treatment resulted in p53 stabilization and target gene activation in CTRL and KDM4A cells (Figures S2H and S2I).

KDM4A-Dependent 1q12h Copy Gain Is Dose Dependent and Requires Catalytic Activity and Tudor Domains

In order to determine whether the expression level and catalytic activity of KDM4A are required for 1q12h copy gain, we overexpressed catalytically active and inactive KDM4A (H188A; Whetstine et al., 2006) with and without KDM4A depletion by shRNA (Figures 3A and S3A). Transient overexpression of KDM4A was sufficient to promote 1q12h copy gain but not alter copy number of Chr 8. However, concomitant depletion of KDM4A suppressed 1q12h gain, which demonstrates the importance of increasing KDM4A levels in order to observe 1q12h gain (Figures 3A and S3A). Importantly, neither catalytically dead KDM4A

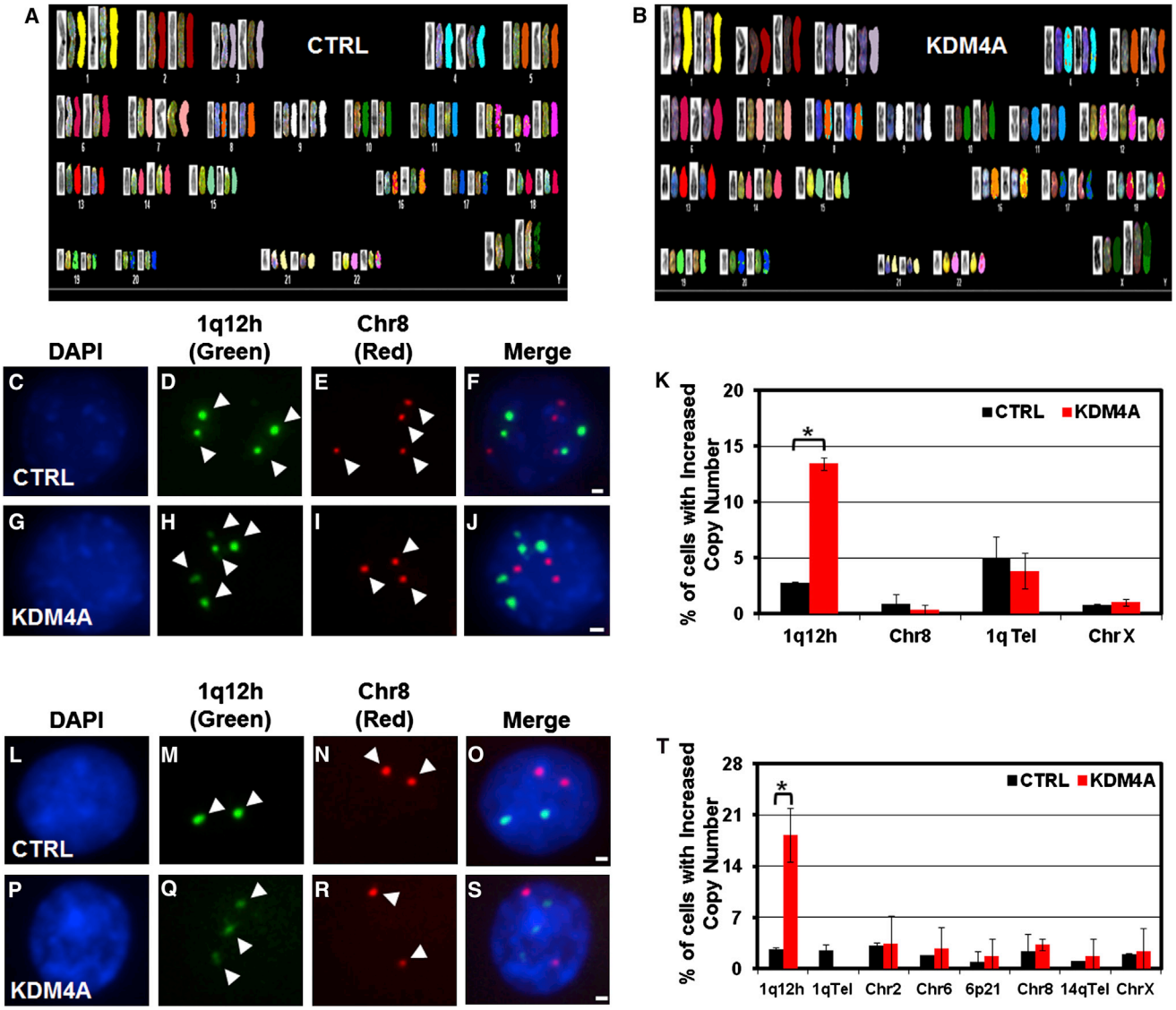

Figure 2. KDM4A Overexpression Results in 1q12h Copy Gain

(A and B) SKY analysis of RPE GFP-CTRL and GFP-KDM4A cells.

(C–J) FISH of stable 293T cells overexpressing GFP-CTRL or GFP-KDM4A, respectively. DAPI, (C) and (G); 1q12h (green), (D) and (H); Chr 8 centromere (red), (E) and (I); merged images in (F) and (J).

(K) Quantification of FISH experiments in stable 293T GFP-CTRL (black bars) and GFP-KDM4A cells (red bars) with the indicated FISH probes.

(L–S) FISH of stable RPE cells overexpressing GFP-CTRL or GFP-KDM4A, respectively. DAPI, (L) and (P); 1q12h (green), (M) and (Q); Chr 8 (red), (N) and (R); merged images in (O) and (S).

(T) Quantitation of RPE FISH experiments.

Arrowheads indicate foci in FISH images. Error bars represent the SEM. Asterisk indicates significant difference from GFP-CTRL ($p < 0.05$) by two-tailed Student's t test. Scale bars, 2 μm. See also Figure S2 and Table S1.

overexpression (Figures 3A and 3B; H188A) nor KDM4A depletion promoted 1q12h copy gain, which emphasizes that the gain is not a dominant-negative effect due to KDM4A overexpression.

We further demonstrated that 1q12h gain occurred in less than 24 hr of KDM4A transient overexpression in RPE cells (Figures 3C, 3D, S3B, and S3C) while not altering copy gain at other regions (Figure 3D). Interestingly, KDM4B, KDM4C, or KDM4D overexpression for 24 hr did not alter 1q12h copy number (Figures 3E and S3C). The copy gain required KDM4A catalytic activity (H188A) and enzymatic domains (JmjC and JmjN; referred to as ΔNC) in RPE cells (Figures 3B, 3C, and S3B). However, the KDM4A catalytic domain alone was insufficient to generate 1q12h gain (Figures 3B and 3C; referred to as NC). Interestingly, the loss of the Tudor domains alone was sufficient to block the 1q12h gain (Figures 3B and 3C; referred to as NCMP). Taken

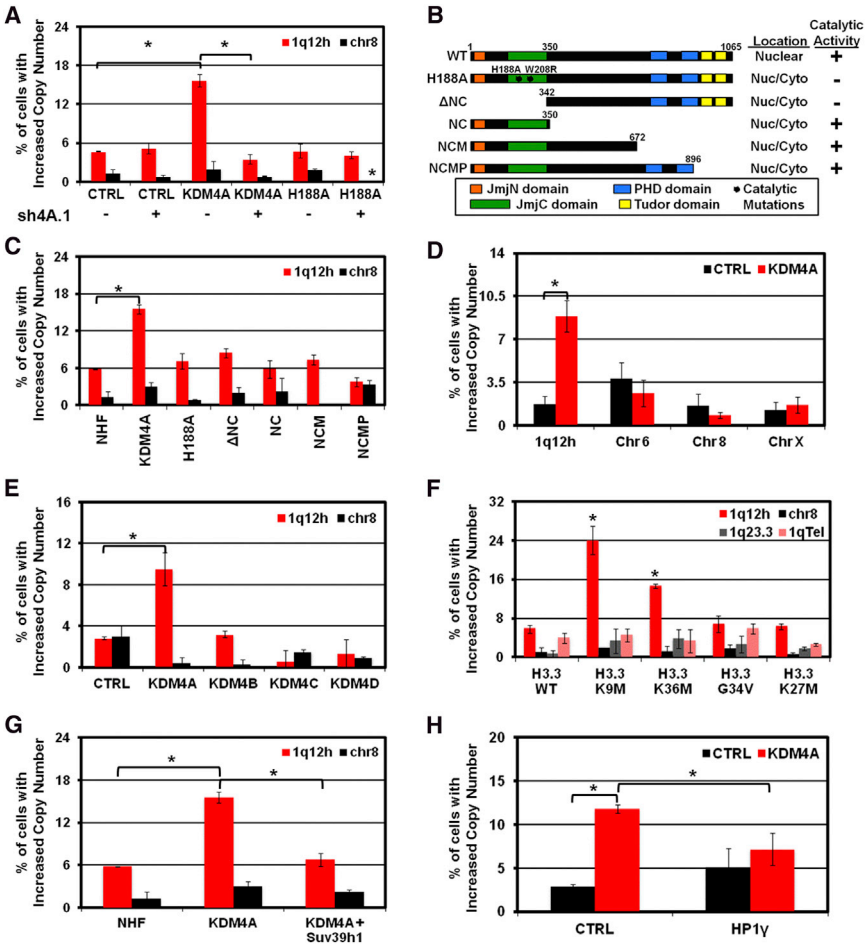

Figure 3. 1q12h Copy Gain Can Be Induced Transiently, Depends on KDM4A Catalytic Activity, and Can Be Antagonized by Suv39h1 and HP1γ

(A) Quantification of FISH experiments in 293T cells overexpressing CTRL, KDM4A, or catalytically inactive KDM4A (H188A) with (+) and without (–) depletion of endogenous KDM4A (sh4A.1) with the indicated FISH probes.

(B) Schematic of NHF-tagged KDM4A constructs. The subcellular localization ("location") occurred in >80% of assayed cells, and catalytic activity ("+") indicates strong reduction in total nuclear H3K36me3.

(C and D) Quantification of FISH experiments with indicated probes in RPE cells transfected for 24 hr with the indicated constructs. (C) NHF-KDM4A constructs. (D) GFP-CTRL (black bars) or GFP-KDM4A (red bars).

(E) 1q12h copy gain is specific to KDM4A overexpression and not other KDM4 family members.

(F) Overexpression of H3.3 histone variants for H3K9 or H3K36 promotes 1q12h gain.

(G and H) Coexpression of Suv39h1 (G) or HP1γ (H) abrogates KDM4A-dependent 1q12h gain.

Error bars represent the SEM. Asterisk indicates significant difference from GFP-CTRL or NHF-CTRL, or H3.3 WT, or comparison indicated by brackets ($p < 0.05$) by two-tailed Student's t test. See also Figure S3.

together, these data emphasize that transient exposure to increased KDM4A levels is sufficient to promote 1q12h copy gain, but this can only occur with a catalytically active enzyme and functional Tudor domains.

Interfering with H3K9 or H3K36 Methylation Promotes 1q12 Copy Gain

The requirement for KDM4A catalytic activity to promote 1q12 copy gain suggests that demethylation of chromatin or a nonhistone target is important for proper regulation of 1q12h ploidy. Recently, Lewis and colleagues demonstrated that H3.3 variants with a methionine in place of the lysine (i.e., H3K27M, H3K9M, and H3K36M) can inhibit EZH2 (K27M), G9a (K9M), and Suv39h1 (K9M), as well as reduce H3K36me3 levels (K36M) (Lewis et al., 2013). Therefore, these H3.3 variants were used to ascertain whether interfering with methylation at any one of these lysines could promote 1q12h copy gain. Each variant was expressed and successfully incorporated into chromatin in 24 hr and reduced the corresponding trimethylation (Figures S3D and S3E). Expression of H3.3 WT, G34V, and H3K27M failed to promote 1q12h copy gain; however, expression of either H3.3K9M or H3.3K36M was sufficient to promote 1q12h gain (Figure 3F; $p = 0.026$ for K9M and $p = 0.006$ for K36M). Furthermore, the 1q12h gain was not caused by a gain of chromosome 1, as there was not an increase in 1q Tel or in the 1q23.3 cytogenetic band midway down the 1q arm (Figure 3F). Because H3.3K9M promoted copy gain at 1q12h and inhibits Suv39h1 (Lewis et al., 2013), we reasoned that overexpression of the H3K9me3 methyltransferase Suv39h1 may suppress KDM4A-dependent copy gain. Consistent with this prediction, coexpression of Halo-Suv39h1 was sufficient to abrogate KDM4A-dependent 1q12h copy gain ($p = 0.0003$ for KDM4A vs NHF; $p = 0.0055$ for KDM4A + Suv39h1 vs KDM4A; and $p = 0.47$ for KDM4A+ Suv39h1 vs NHF) (Figures 3G and S3F). These results highlight the importance of methylation in modulating site-specific copy gain, especially the lysines that are substrates for KDM4A.

HP1γ Antagonizes KDM4A-Dependent Increased 1q12 Copy Number

KDM4A-dependent changes in cell-cycle progression and replication timing at Chr1 sat2 are antagonized by HP1γ overexpression (Black et al., 2010). Therefore, we hypothesized that HP1γ overexpression could antagonize the increased copy number of 1q12 in KDM4A-overexpressing cells. Cotransfection of HP1γ reduced the 1q12h copy gain to levels comparable to that seen in control cells ($p = 0.29$ for KDM4A + HP1γ vs GFP-CTRL+ HP1γ; and $p = 0.009$ for KDM4A + HP1γ vs KDM4A + RFP-CTRL) (Figures 3H and S3G). Surprisingly, transfection of HP1γ into RPE cells stably overexpressing KDM4A or stably co-overexpressing HP1γ and KDM4A did not reverse

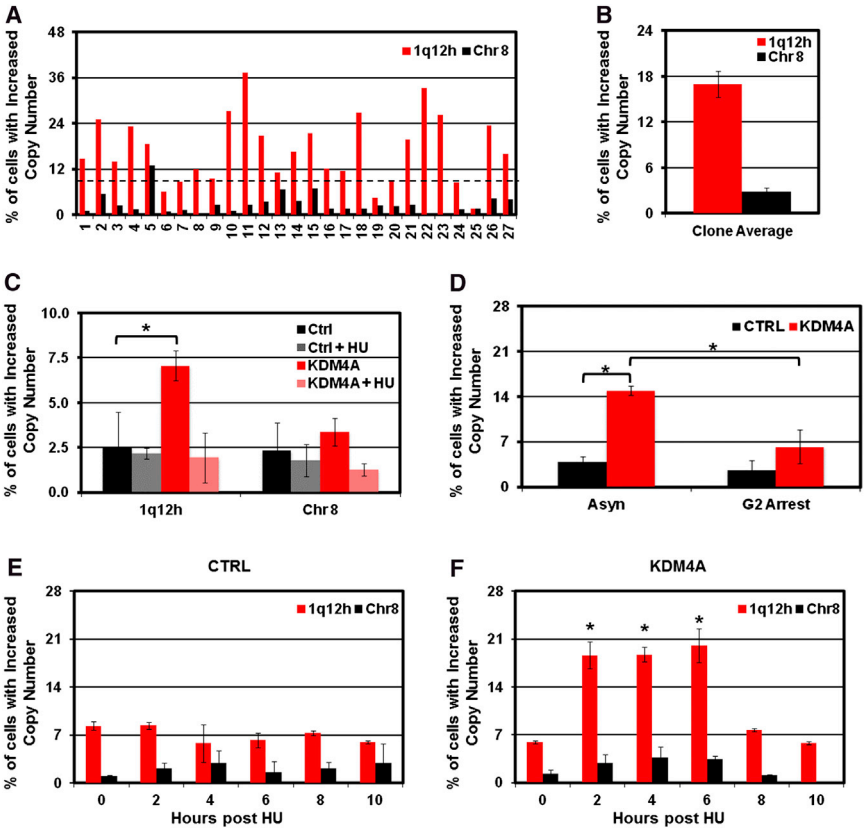

Figure 4. 1q12h Copy Gain Is Not Stably Inherited and Requires S Phase Each Cell Cycle

(A) Increased 1q12h copy number in GFP-KDM4A RPE cells is not inherited. FISH of single-cell clones derived from RPE KDM4A cells.

(B) Average copy gain for 27 single-cell clones from (A) is graphically depicted.

(C) Increased copy number of 1q12h requires S phase.

(D) 1q12h gain is lost by the end of G2.

(E and F) 1q12h copy gain is generated in S phase. Stable GFP-CTRL (E) and GFP-KDM4A (F) RPE cells were arrested in hydroxyurea (HU) for 20 hr and released for the time indicated prior to FISH analysis.

Error bars represent the SEM. Asterisk indicates significant difference from GFP-CTRL or comparison indicated by bracket ($p < 0.05$) by two-tailed Student's t test. For the HU release, p values are based on the comparison of KDM4A to CTRL at each individual time point (F and E, respectively). See also Figure S4.

the increased copy number of 1q12h (data not shown). These results imply that, once an altered chromatin conformation is established, HP1γ is insufficient to restore proper regulation of 1q12 copy number in KDM4A overexpressing cells.

1q12 Copy Gain Is Not Stably Inherited and Requires S Phase

Because KDM4A overexpression promotes 1q12 gain, we asked whether the increased copy number was stably inherited or was regenerated during subsequent cell cycles. First, single-cell clones were established from our stably overexpressing KDM4A RPE cell line and were assayed by 1q12h FISH (Figure 4A). If the copy number of 1q12h was stably inherited, some clones should have 100% of cells with 1q12h copy gain. Instead, we observed a distribution of copy gain between 1.5% and 37%, which supports the model that 1q12 gain is most likely not stably inherited (Figures 4A and S4A). The clones lacking increased copy of 1q12h (below black dashed line) no longer overexpressed KDM4A (Figure S4A). Furthermore, the average of all clones assayed was 17.0%, agreeing with our analysis of the starting stable population (Figures 4B and 2T, respectively).

We next investigated whether stably overexpressing KDM4A RPE cells gain extra copies of 1q12h during each cell division. The 1q12h copy gain was eliminated in KDM4A overexpressing RPE cells arrested in G1/S with HU (Figures 4C and S4B). Because apoptosis was not increased in asynchronous or HU-arrested KDM4A cells, the lack of copy gain was not due to increased apoptosis removing cells with extra 1q12h (Figure S4C). However, doxorubicin treatment could induce apoptosis in both CTRL and KDM4A cells, which was significantly reduced in KDM4A-overexpressing cells (Figure S4C). We then tested whether 1q12h gain persisted through G2 by arresting cells in late G2 with the CDK1 inhibitor R03306 (Figure S4B; Vassilev, 2006). KDM4A cells arrested in late G2 and did not display 1q12h copy gain (Figure 4D).

Given that KDM4A-dependent 1q12h copy gain did not occur during G1/S or G2 arrest, we hypothesized that KDM4A promotes copy gain during S phase. In agreement with this hypothesis, GFP-KDM4A cells, but not GFP-CTRL cells, were able to promote additional copies of 1q12h, but not Chr 8 centromere following HU release (Figures 4E and 4F). The additional copies occurred between 2 and 6 hr post-HU release and were lost between 8 and 10 hr following release. Taken together, our data support a model whereby KDM4A promotes copy gain of specific chromosomal regions during S phase, which are then eliminated by the end of the G2 phase of cell cycle.

KDM4A Associates with Replication Machinery and Promotes Rereplication of 1q12

In order to gain molecular insight into how KDM4A is involved in generating 1q12h copy gain, we identified KDM4A-interacting proteins by performing mass spectrometry analysis of proteins interacting with Halo-KDM4A. We observed a significant enrichment for proteins involved in replication using IPA (Figure 5A; $p = 0.00000795$). Interestingly, many of these proteins are required for rereplication (e.g., MCMs and DNA polymerases; Arias and Walter, 2007; Snaith and Forsburg, 1999).

Previous work verified KDM4A associations with cullin 1 (Van Rechem et al., 2011) and p53 (Kim et al., 2012). We further validated additional interactions by conducting endogenous

A

	HALO-KDM4A Purification							
	Peptide Count				NSAF			
Gene Symbol	KDM4A-1	Control-1	KDM4A-2	Control-2	KDM4A-1	Control-1	KDM4A-2	Control-2
MCM3	41	3	42	0	1.50E-03	2.70E-04	1.58E-03	0.00E+00
MCM4	5	0	7	0	1.72E-04	0.00E+00	2.47E-04	0.00E+00
MCM5	25	0	29	0	1.02E-03	0.00E+00	1.21E-03	0.00E+00
MCM7	12	0	18	0	4.94E-04	0.00E+00	7.62E-04	0.00E+00
CACYBP	23	0	28	0	2.95E-03	0.00E+00	3.69E-03	0.00E+00
CDK1	9	0	15	0	8.83E-04	0.00E+00	1.51E-03	0.00E+00
CUL1	60	0	41	0	2.22E-03	0.00E+00	1.56E-03	0.00E+00
DDB1	48	0	50	0	1.26E-03	0.00E+00	1.35E-03	0.00E+00
DNAJA3	16	0	10	0	1.01E-03	0.00E+00	6.47E-04	0.00E+00
DUT	6	0	5	0	7.41E-04	0.00E+00	6.35E-04	0.00E+00
HUWE1	21	2	19	0	1.45E-04	3.40E-05	1.35E-04	0.00E+00
RFC2	9	0	17	0	7.70E-04	0.00E+00	1.49E-03	0.00E+00
RFC4	6	0	13	0	5.00E-04	0.00E+00	1.11E-03	0.00E+00
RFC5	15	0	17	0	1.32E-03	0.00E+00	1.53E-03	0.00E+00
POLA1	10	0	8	0	2.01E-04	0.00E+00	1.65E-04	0.00E+00
POLD1	5	0	7	0	1.34E-04	0.00E+00	1.93E-04	0.00E+00
POLE	7	0	16	0	8.91E-05	0.00E+00	2.09E-04	0.00E+00
SSBP1	14	0	14	0	2.75E-03	0.00E+00	2.82E-03	0.00E+00
TP53	7	0	13	0	5.31E-04	0.00E+00	1.01E-03	0.00E+00
TRRAP	37	0	27	0	2.82E-04	0.00E+00	2.11E-04	0.00E+00
UPF1	6	0	11	0	1.61E-04	0.00E+00	3.04E-04	0.00E+00
WRNIP1	5	0	11	0	2.32E-04	0.00E+00	5.24E-04	0.00E+00

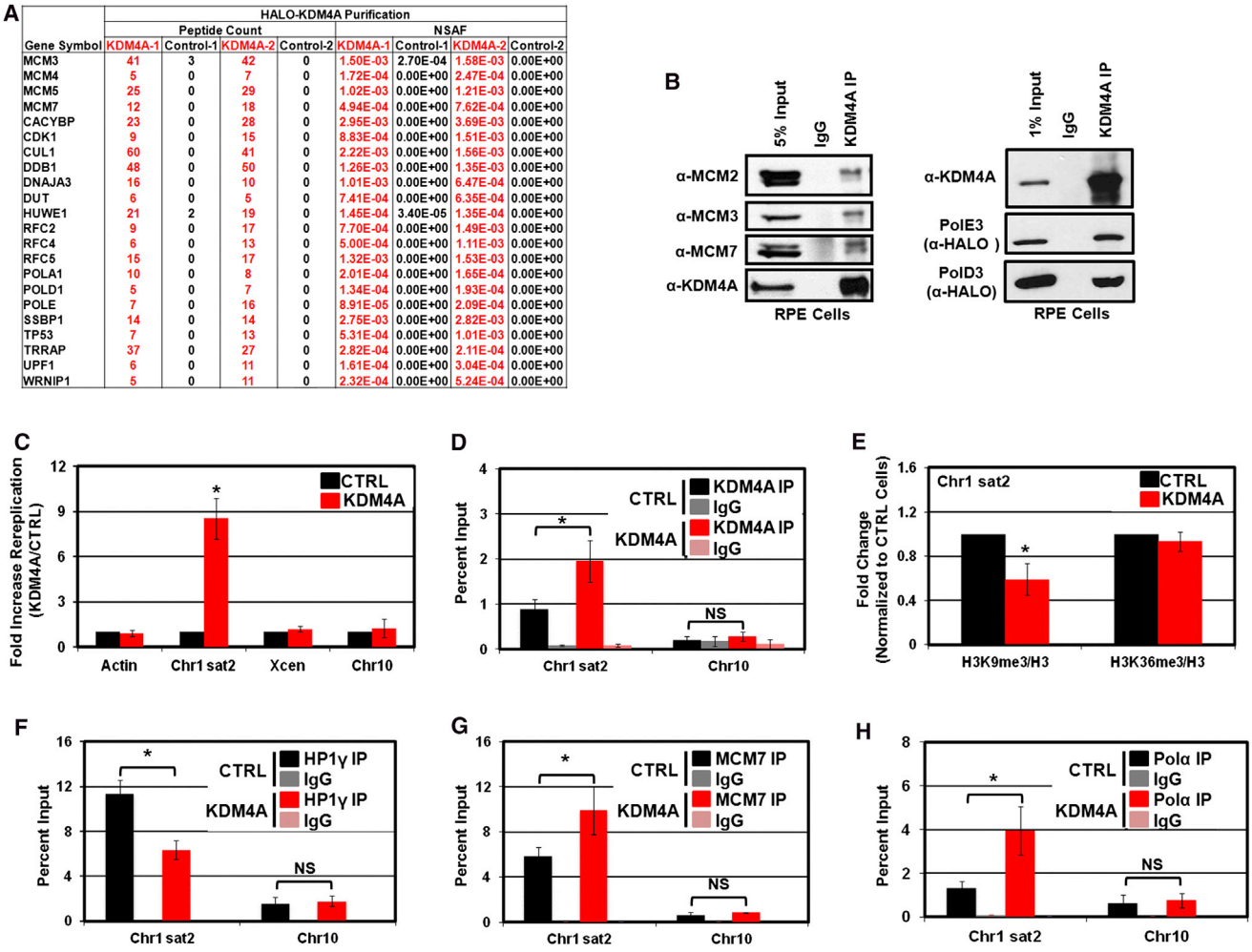

Figure 5. KDM4A Interacts with Replication Machinery, and KDM4A Overexpression Promotes Rereplication

(A) Table depicting mass spectrometry analysis of KDM4A-interacting proteins related to replication.

(B) Western blots of coimmunoprecipitation of endogenous KDM4A and the indicated licensing and replication machinery in RPE Cells.

(C) KDM4A overexpression in RPE cells leads to rereplication of Chr1 sat2.

(D) KDM4A is enriched at Chr1 sat2 (1q12) in HU-arrested KDM4A-overexpressing RPE cells.

(E) H3K9me3, but not H3K36me3, decreases at Chr1 sat2 in HU-arrested cells.

(F) HP1γ enrichment decreases at Chr1 sat2 (1q12) in HU-arrested KDM4A-overexpressing cells.

(G and H) MCM7 and DNA polymerase α (Pol α) are enriched at Chr1 sat2 (1q12) in HU-arrested KDM4A-overexpressing cells.

Error bars represent the SEM. Asterisk indicates significant difference from GFP-CTRL or comparison indicated by bracket ($p < 0.05$) by two-tailed Student's t test. See also Figure S5.

KDM4A coimmunoprecipitation with MCM2, MCM3, and MCM7 or Halo-tagged DNA polymerase subunits (Figures 5B and S5A). Although MCM2 was not identified in our mass spectrometry analysis, it associated with KDM4A, suggesting that the entire MCM complex interacts with KDM4A.

Because KDM4A overexpression promoted copy gain in a replication-dependent manner and interacted with DNA polymerases and the replication licensing machinery, we hypothesized that KDM4A overexpression was promoting rereplication within 1q12. To test this hypothesis, we utilized cesium chloride density gradient centrifugation (Figure S5B). Our labeling procedure was performed for less than one complete cell cycle, producing an enrichment in heavy-light (H:L)-replicated DNA while still maintaining an unreplicated light-light fraction (L:L). We did not detect a peak of enrichment of H:H DNA, indicating that KDM4A overexpression does not promote widespread rereplication, as seen with other chromatin regulators (KMT5A; Tardat et al., 2010). We pooled and purified the fractions in which the H:H DNA should separate and then assayed the rereplicated DNA for specific regions. Because Chr1 sat2 resides in 1q12 (Wong et al., 2001) and is bound and modulated by KDM4A, we reasoned that it could be a rereplicated target. We observed a 7-fold enrichment of Chr1 sat2 in the rereplicated fraction from KDM4A-overexpressing cells, whereas the β-actin locus and a region near the X centromere, which we previously reported as a KDM4A target (Black et al., 2010), were not enriched (Figures

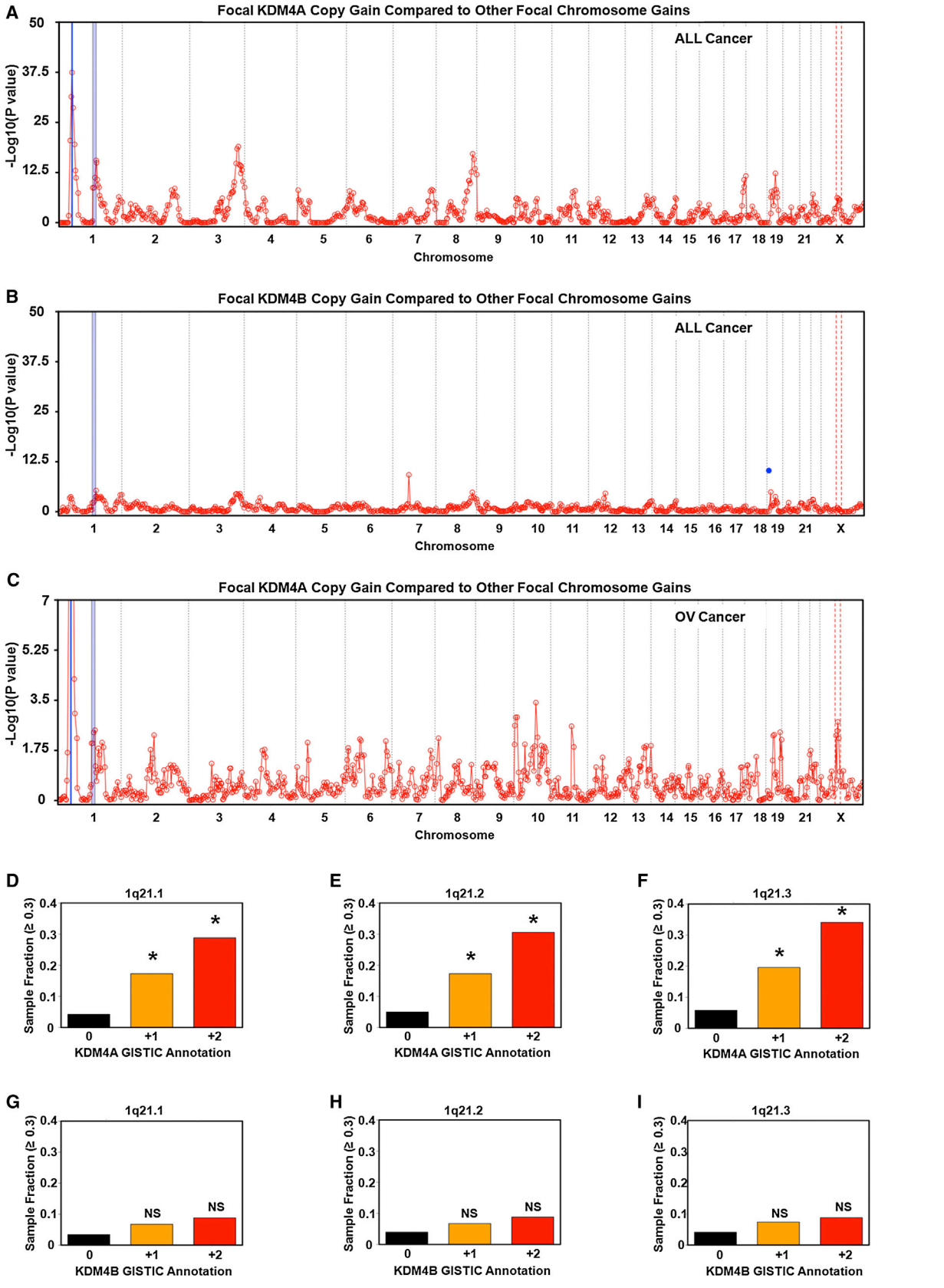

(legend on next page)

5C and S5C). The enrichment in Chr1 sat2 rereplication represented a small amount of the input DNA and was consistent with a subpopulation of cells generating and losing the 1q12h copy gain (Figure S5C). Taken together, our data demonstrate that KDM4A associates with replication proteins and promotes rereplication at a specific locus that exhibits copy gains.

KDM4A Overexpression Promotes Chromatin State Changes and Recruitment of Replication Machinery

Our data support a model whereby KDM4A overexpression promotes methylation changes, displacement of HP1γ, and recruitment of replication machinery to specific genomic regions, resulting in rereplication. To test this model, we performed ChIP experiments to evaluate methylation levels, HP1γ enrichment, and replication machinery occupancy at Chr1 sat2. As a negative control, we identified an intergenic region on chromosome 10 (Chr10) that is acetylated at H3K9 in numerous cell types (according to UCSC browser; data not shown) that should not be enriched for H3K9me3 or KDM4A. KDM4A overexpression increased KDM4A recruitment to Chr1 sat2, but not Chr10 (Figure 5D), which corresponded to a loss of H3K9me3 and HP1γ depletion (Figures 5E and 5F). We did not observe any change in H3K36me3 at Chr1 sat2, which was consistent with our previous findings in 293T cells (Black et al., 2010). Finally, both MCM7 and Polα were enriched at Chr1 sat2, but not at Chr10, upon KDM4A overexpression (Figures 5G and 5H, respectively). Our data demonstrate that KDM4A overexpression promotes H3K9me3 and HP1γ loss, increased replication machinery recruitment, and rereplication.

Identification of Regions Coamplified with KDM4A in Cancer

To identify additional regions that have copy gains upon KDM4A overexpression, we determined whether *KDM4A* focal amplification (1p34.2) in primary tumors was correlated with copy gains of any of the 807 cytogenetic bands in 4,420 tumor samples (Figure 6A, which represents 19 tumor types, including the 8 analyzed in Figure S1). We observed correlated copy gains from 1p11.2 through 1q21.3 on chromosome 1 in two independent statistical tests (Figures 6A and S6A, blue shading; see Experimental Procedures). Due to the minimal sequence annotation and repetitive nature of 1q12, we did not calculate a correlation for this cytogenetic band. However, the cytogenetic bands immediately flanking 1q12 (1p11.2 and 1q21.1) exhibited cogain with *KDM4A* amplification, which suggests that 1q12 is likely coamplified in these tumors. These coamplified regions were specific to *KDM4A* because there was not a strong correlation when the identical analysis was performed with respect to *KDM4B* coamplification (Figures 6B and S6B). We observed that individual coamplified regions could universally be observed, whereas others could be differentially regulated in a tumor- and/or tissue-specific manner. For example, the ovarian cancer data sets demonstrated coamplification with 1p11.2-1q21.3, whereas some *KDM4A*-coamplified regions were lost (e.g., the region on 17q positions 17q24.2 to 17q25.3) and others were enhanced (e.g., the region on X chromosome positions Xp11.2 to Xq13.2) in the ovarian cancer profile (Figures 6C and S6C).

Next, we tested whether gains in 1q21.1-1q21.3 were affected by the amplification level of *KDM4A* (Figures 6D–6F and S6D–S6F). Indeed, when *KDM4A* had a high-level focal amplification (GISTIC +2), a significantly greater fraction of samples were amplified in 1q21.1-1q21.3 compared to cases in which *KDM4A* was not amplified (GISTIC 0; Fisher's exact test; $p = 2 \times 10^{-9}$ in 1q21.1, 1.9×10^{-9} in 1q21.2, and 1.02×10^{-10} in 1q21.3) (Figures 6D–6F). When comparing lower-level amplification of *KDM4A* (GISTIC +1) to the *KDM4A*-unamplified cases, we observed a reduced sample fraction but still highly significant amplification of 1q21.1-1q21.3 ($p = 2.04 \times 10^{-25}$ in 1q21.1, 6.28×10^{-22} in 1q21.2, and 3×10^{-24} in 1q21.3). In contrast, when stratifying the samples based on *KDM4B* amplification status (Figures 6G–6I and S6G–S6I), the differences are not significant (all p values > 0.1 by Fisher's exact test), although a minimal trend in the same direction is observed. These results demonstrate that *KDM4A* amplification in tumors correlated with amplification of specific cytogenetic bands, which suggests that KDM4A may promote site-specific copy gains in vivo.

Copy Gain and Rereplication Occur in Regions Coamplified in Tumors

Because 1q21.1-1q21.3 amplification correlated with *KDM4A* amplification, we assessed whether these regions were gained by FISH and rereplicated by density gradient centrifugation in transgenic cell lines. We observed increased copy number of 1q12 through 1q21.2 in our KDM4A-overexpressing cells, but not in control cells (Figures 7A and 7B). Our coamplification

Figure 6. Identification of Cytogenetic Bands Coamplified with KDM4A in Cancer

(A) Focal amplification of cytogenetic bands correlates with amplification of *KDM4A* in cancer. The blue line represents the locus of *KDM4A*, and its gene-specific significance is $p = 1.5 \times 10^{-37}$.

(B) Focal amplification of cytogenetic bands with amplification of *KDM4B*. The blue dot represents the gene-specific significance of *KDM4B*.

(C) Focal amplification of cytogenetic bands correlates with amplification of *KDM4A* in 547 ovarian cancer samples. The blue line represents the locus of *KDM4A*, and its gene-specific significance is $p = 1.1 \times 10^{-19}$. For each coamplification plot, blue shaded regions indicate 1p11.2 through 1q21.3, and red dashed lines indicate Xp11.2 through Xq13.2.

(D) Increased copy of *KDM4A* is associated with increased mean focal copy of 1q21.1 $p = 2 \times 10^{-9}$ for +2 versus 0 and $p = 2.04 \times 10^{-25}$ for +1 versus 0 by Fisher's exact test.

(E) Increased copy of *KDM4A* is associated with increased copy of 1q21.2 ($p = 1.9 \times 10^{-9}$ for +2 versus 0 and $p = 6.28 \times 10^{-22}$ for +1 versus 0).

(F) Increased copy of *KDM4A* is associated with increased copy of 1q21.3 ($p = 1.02 \times 10^{-10}$ for +2 versus 0 and 3×10^{-24} for +1 versus 0).

(G) Increased copy number of *KDM4B* is not associated with increased copy of 1q21.1 ($p = 0.18$ for +2 versus 0).

(H) Increased copy number of *KDM4B* is not associated with increased copy of 1q21.2 ($p = 0.22$ for +2 versus 0).

(I) Increased copy number of *KDM4B* is not associated with increased copy number of 1q21.3 ($p = 0.24$ for +2 versus 0).

Asterisk indicates significant difference of +1 or +2 versus 0 by Fisher's exact test. NS, not significantly different than 0. See also Figure S6.

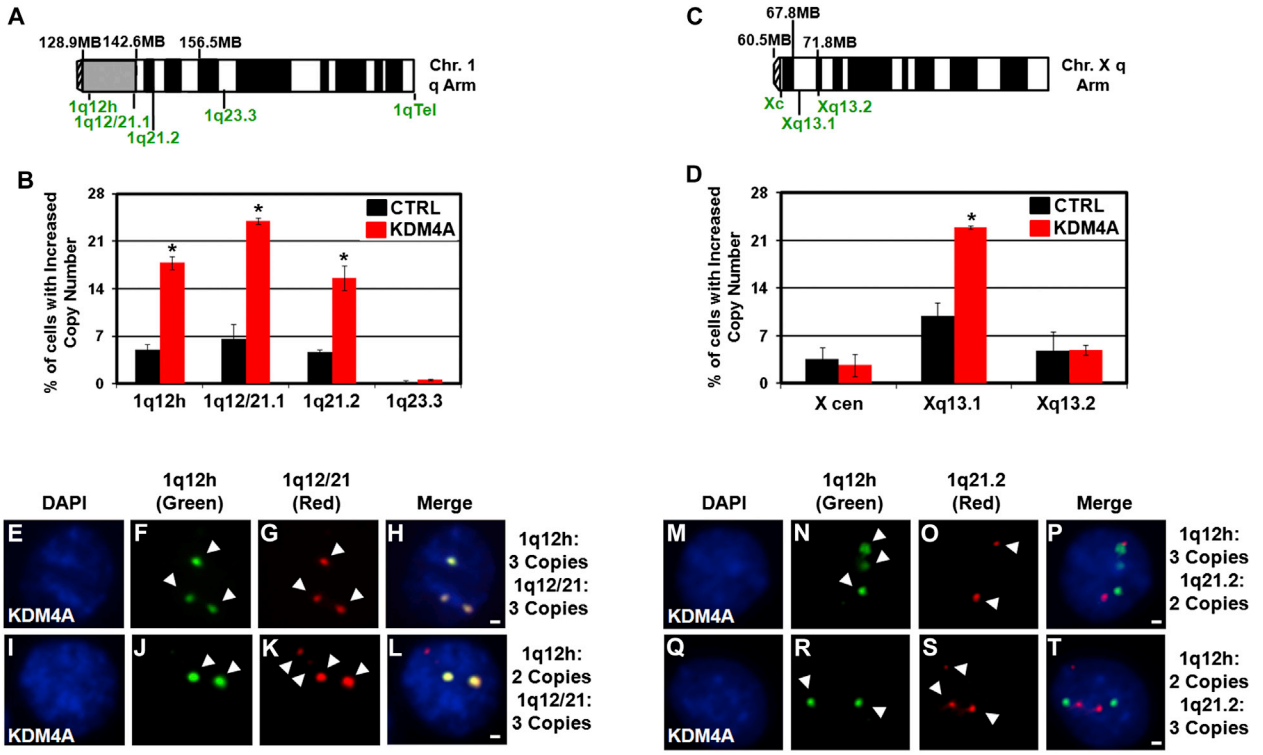

U

Distribution of copy gain of 1q12h and 1q12/21.1 in KDM4A Overexpressing Cells			
	3x3	3x2	2x3
KDM4A	65.96%	2.13%	31.91%
% of Cells with 1q12h and 1q21.2 Foci			
	3x3	3x2	2x3
KDM4A	8.16%	50.00%	41.84%

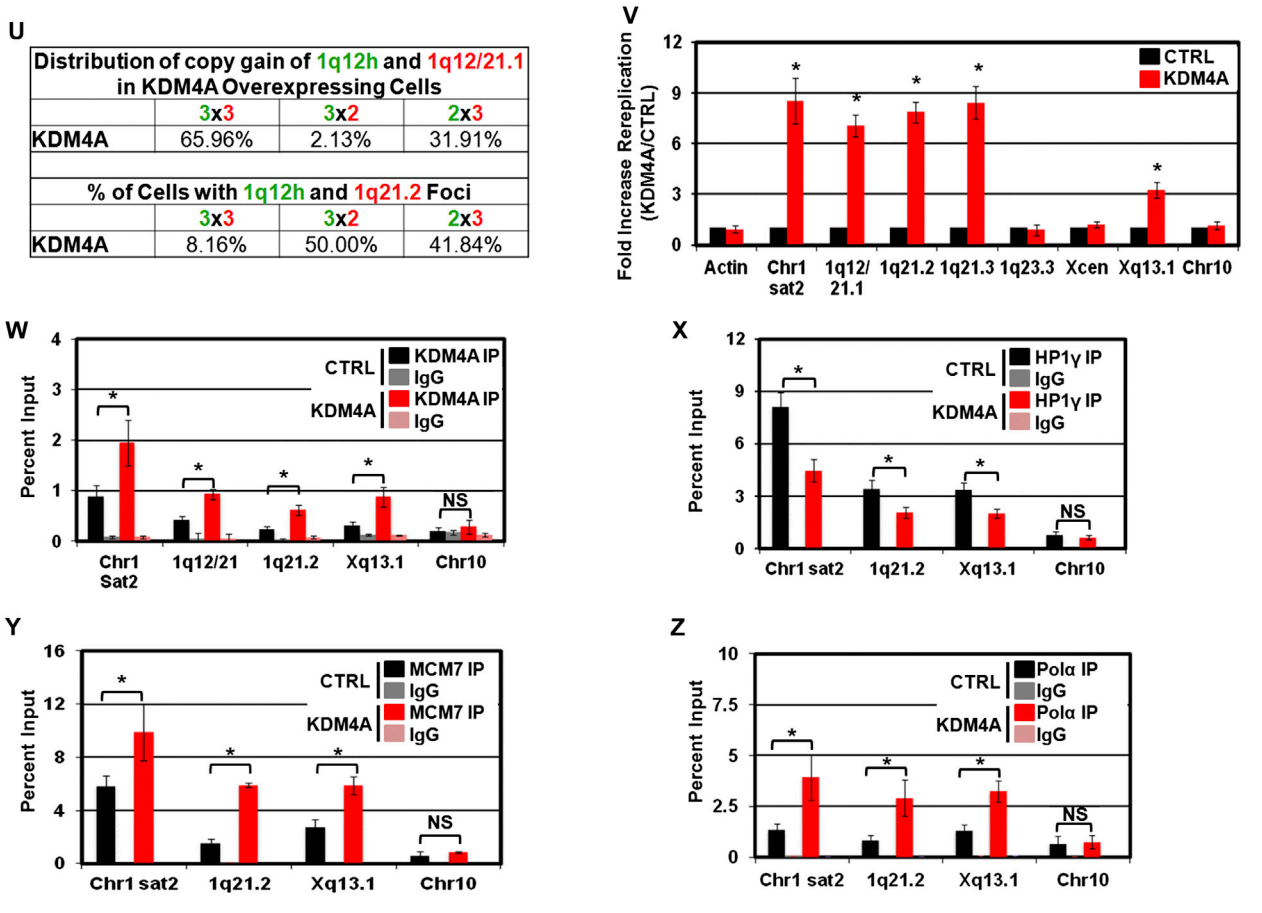

(legend on next page)

analysis of all tumors indicated that the correlation with *KDM4A* copy number diminished at 1q23.3, suggesting that 1q23.3 is not amplified in KDM4A-overexpressing cells, which was in fact the case in KDM4A-overexpressing RPE cells (Figures 7A and 7B).

We then evaluated copy gain of other chromosomal domains identified through our coamplification analysis. We chose to examine the small focal peak on the X chromosome (Xp11.2-Xq13.2), which was specific to coamplification with *KDM4A* across all cancers and was even more enriched in ovarian cancer (Figures 6A and 6C, respectively). KDM4A-overexpressing RPE cells exhibited Xq13.1 copy gains, but not the X centromere or Xq13.2 (Figures 7C and 7D). Xq13.1 as well as 1q12/21 and 1q21.2 copy gains were also observed in 293T cells overexpressing KDM4A (Figure S6J). These data demonstrate that *KDM4A*-coamplified regions in primary tumors are generated by KDM4A overexpression in transgenic cell lines.

The coamplification analysis of tumor data sets does not distinguish whether the entire intervening sequence between 1q12h and 1q21.3 was amplified in the same tumor cells. Therefore, we scored the 1q12/21 or 1q21.2 FISH probes with the 1q12h probe in the same KDM4A-overexpressing cells (Figures 7A and 7E–7U). We observed that approximately two-thirds of the KDM4A-overexpressing cells with 1q12h amplification also had 1q12/21.1 amplification, whereas approximately one-third had only 1q12/21.1 copy gain but lacked 1q12h gain (Figure 7U). In the case of 1q12h or 1q21.2 amplification, the majority of cells had gains in one or the other cytogenetic band (Figures 7M–7U). Taken together, these data demonstrate that the entire region between 1q12h and 1q21.3 is not contiguously amplified but that KDM4A is directing copy gain within these cytogenetic bands. The ability to detect nonoverlapping foci also suggests that the additional copies may exist as extrachromosomal pieces. This possibility was further supported by the fact that 1q12/21 FISH marked the additional 1q12/21 copy adjacent to or physically distinct from the chromosome 1 painted territory (Figures S7A–S7L).

To address whether these gained regions were through rereplication, we assayed our CsCl gradient H:H fraction for regions under our FISH probes in the indicated cytogenetic bands (Figure 7V). We observed rereplication at 1q12h (indicated by Chr1 sat2), 1q12/21.1, 1q21.2, and 1q21.3, but not in 1q23.3 or on Chr10. Rereplication was detected inside Xq13.1, but not near the X centromere. In addition, the rereplicated regions were bound by KDM4A, which was further enriched upon KDM4A overexpression (Figures 7W and S6K). As with Chr1 sat2, KDM4A overexpression promoted loss of HP1γ (Figure 7X) and recruitment of MCM7 and Polα to 1q21.2 and Xq13.1 (Figures 7Y and 7Z, respectively). Taken together, our data are consistent with the model that KDM4A overexpression promotes copy gain and rereplication at specific sites within the genome in vivo (tumors) and in vitro (transgenic cell lines).

DISCUSSION

Genomic instability is a major contributing factor to the development and onset of age-related diseases. Cancer cells often contain alterations in copy number of genes, specific genomic regions, chromosome arms, and entire chromosomes. However, the underlying molecular mechanisms that lead to these copy number alterations are poorly understood. Here, we report that overexpression of a single chromatin modifying enzyme, KDM4A, is sufficient to promote rereplication and copy gain of specific chromosomal domains. Furthermore, KDM4A-dependent amplified regions are found coamplified with *KDM4A* in primary tumors. Our results support a model in which increased expression of KDM4A promotes recruitment of KDM4A to specific genomic regions and promotes rereplication (Figure S7M).

KDM4 Members and Cancer

Our results demonstrate that *KDM4A* is amplified in different tumor types and correlates with increased *KDM4A* expression. Intriguingly, when compared to other tumor types, ovarian cancer is enriched for amplifications of *KDM4A*, which correlate with poor outcome in these cases. Levels of KDM4A may therefore represent a good biomarker for ovarian cancer, especially with respect to novel therapies that target this lysine demethylase. In addition, ovarian patients with increased levels of KDM4A may respond more poorly to S-phase chemotherapeutics, as KDM4A overexpression resulted in better recovery from HU (Black et al., 2010). Consistent with this possibility, ovarian cell lines with 1q12-21 amplification are often more resistant to cisplatin treatment (Kudoh et al., 1999; Takano et al., 2001). Interestingly, drug resistance in multiple myeloma is also associated with 1q12-21 amplification (Inoue et al., 2004). Addressing the relationship between KDM4A, 1q12-21 coamplification, and drug responses will be important in future studies.

Figure 7. KDM4A Overexpression Leads to Copy Gains and Rereplication of Regions Coamplified in Tumors

(A) Chromosome arm schematic depicting location of FISH probes used on chromosome 1.

(B) KDM4A overexpression increased copy number of 1q12h, 1q12/21.1, and 1q21.2, but not 1q23.3.

(C) Chromosome arm schematic depicting location of FISH probes used on chromosome X.

(D) KDM4A overexpression increases copy number of Xq13.1, but not X cen or Xq13.2 in RPE cells.

(E–T) FISH of stable RPE cells overexpressing GFP-CTRL or GFP-KDM4A with indicated FISH probes.

(U) Table summarizing coamplification of 1q12h, 1q12/21.1, and 1q21.2 in (E)–(T). Data are presented as percentage of amplified cells having 2 or 3+ copies of the indicated FISH probes.

(V) KDM4A-dependent rereplication of chromosomal domains.

(W) KDM4A ChIP in HU-arrested cells. KDM4A is enriched in rereplicated regions in KDM4A-overexpressing RPE cells.

(X) HP1γ enrichment decreases at rereplicated regions in KDM4A-overexpressing cells following 1 hr release from HU arrest.

(Y and Z) MCM7 and DNA polymerase α (Pol α) are enriched at rereplicated regions in HU-arrested KDM4A-overexpressing cells, respectively.

Error bars represent the SEM. Asterisk indicates significant difference from GFP-CTRL or comparison indicated by bracket ($p < 0.05$) by two-tailed Student's t test. For rereplication (V) and ChIP experiments (W–Z), Chr1 sat2 and Chr10 are the data presented in Figure 5 for reference. Scale bars, 2 μm.

See also Figures S6 and S7.

Even though KDM4 family members have a high degree of homology, they have different distribution of genomic anomalies in cancer. We observed focal deletions in *KDM4B-D*, whereas none were observed in *KDM4A* across the eight different tumor types (Figures S1A–S1D). We also found that KDM4A was the only family member that had a correlation between focal amplification and poor outcome for ovarian cancer patients. Thus, it is intriguing to speculate that KDM4 family enzymes may play different roles in ovarian cancer and other tumor types. Overall, our data highlight the idea that these family members are not created equal but, most likely, have their own specific roles in cancer and in other diseases.

Chromatin Environment and KDM4A-Dependent Copy Gain

Work in yeast demonstrates that specific genomic regions can generate extra DNA fragments in S phase, which depends on the chromatin environment (Kiang et al., 2010). These observations are consistent with our KDM4A-dependent rereplication of specific chromosomal regions. These regions are enriched for KDM4A binding upon overexpression of KDM4A, rereplicate, and have increased copy number during S phase. Interestingly, not all KDM4A-occupied sites are rereplicating in the cell lines tested (Figure 7V). However, this could reflect the chromatin environment in these particular cells or distinct chromatin states influenced by other chromatin modifiers. This would be consistent with our ability to see Xq13.1 and X centromere copy gain in *KDM4A* focally amplified tumors while only seeing the copy gain and rereplication of Xq13.1 in our transgenic cell lines. Thus, different genomic regions may be susceptible to KDM4A-dependent rereplication in specific tissue types.

Consistent with the model that chromatin state impacts copy gain, we demonstrated that interfering with H3K9 or K36 methylation resulted in the site-specific gain of 1q12h in 24 hr, whereas overexpression of Suv39h1 or HP1γ was able to suppress the 1q12h gain. Surprisingly, we were unable to reverse KDM4A-dependent copy gains in cells stably overexpressing KDM4A by overexpressing HP1γ even though these copy gains are regenerated each cell cycle. This observation supports a model whereby KDM4A may establish a chromatin state that promotes rereplication and increased copy number of specific chromosomal regions. Formation of this chromatin state could be antagonized by HP1γ, but not reversed once established. Taken together, these data strongly suggest that the reader, the lysine, and the KDM/KMT balance are required to maintain regulation at these regions. Therefore, we hypothesize that the local chromatin environment will be an important determinant in designating whether certain regions are more susceptible to copy gains and rereplication (see Figure S7M). Based on our observations, we also believe that other methyltransferases or chromatin modulators (e.g., readers or remodelers) may be able to block or reset the established chromatin state in KDM4A-overexpressing cells or that these modulators may have their own independent roles in regulating site-specific copy gains.

KDM4A and Rereplication

Increased KDM4A occupancy promotes a more open chromatin environment through decreasing H3K9me3 and HP1γ occupancy (Figure S7M; Black et al., 2010). KDM4A overexpression also promotes recruitment of the replication licensing machinery and DNA polymerases to sites of rereplication and copy gain (Figure S7M, model). Because copy gains require the KDM4A Tudor domains, we favor the model that KDM4A directly increased chromatin accessibility and, in turn, loading of the MCM and replication complex on chromatin (Figure S7M). This loading and rereplication could occur in the absence of CDT1, CDC6, and ORC, as they are not necessary for replication after MCMs have been successfully loaded (Arias and Walter, 2007). However, the more open chromatin could independently promote inappropriate recruitment of MCMs and DNA polymerases to unused or reused origins, thus promoting rereplication (Figure S7M). This later model would be consistent with the observation that interfering with H3K9 or K36 methylation can promote the site-specific gain in cells with wild-type KDM4A levels. Regardless of the exact details, the data presented in this study support the model that alterations of heterochromatin and methylation at specific regions are more prone to rereplication and, in turn, copy gain.

KDM4A and Extrachromosomal DNA

Because the extra copies of 1q12 are not inherited but are removed prior to completion of G2, it is likely that such regions exist as extrachromosomal DNA (Figures S7H and S7L). As such, it is possible that KDM4A is promoting rereplication at regions that promote head-to-tail collision of one replication fork chasing another (Figure S7M). This model fits a previous study showing that deregulation of replication licensing promotes DNA fragmentation and was consistent with fork collision (Davidson et al., 2006). The presence of these fragments could also explain why KDM4A-overexpressing cells exhibit a moderate increase in p53 stabilization (Figure S2H); that remains below the threshold required to elicit the p53 checkpoint (Kracikova et al., 2013). It is also possible that site-specific rereplication may not be restricted to cancer cells. Transiently upregulating enzymes that direct site-specific rereplication to increase copy number of specific genes may be a general mechanism to allow cells the plasticity to respond to developmental, environmental, or stress conditions without altering their genetic makeup.

KDM4A-Dependent Transient Copy Gain

Because transient KDM4A overexpression was sufficient to promote localized changes in copy number in a single cell cycle, the amplification of specific regions may precede genetic changes in tumors. For instance, transient misregulation of chromatin regulators by altered environmental factors, metabolic changes, hypoxia, or miRNAs could lead to temporary changes in copy number of small genomic regions. If these regions contain oncogenes, this could create a feedback loop that promotes tumorigenesis while masking the originating event (e.g., transient upregulation of KDM4A). Of note, several putative oncogenes reside in the 1q12 and 1q21 cytogenetic bands, including *BCL9* and *MCL1*. In fact, KDM4A binds the *BCL9* locus and causes both copy gain and rereplication of this site (1q21.2 region, Figures 7W and 7V, respectively). However, we do not observe increased expression of Bcl9, which likely reflects the

lack of additional stimulus, transcription factors, or the low percentage of cells with this particular copy gain (data not shown).

It remains unclear how the rereplicated regions are removed as cells exit S phase and enter G2/M. It is possible that cells possess an active method for degradation or removal of these regions. Understanding the events leading to removal of inappropriately amplified regions could be critical to helping to identify pathways that may be misregulated in cancer and lead to the accumulation and inheritance of copy number changes. We hypothesize that other events could then promote incorporation of these transiently amplified regions and, in turn, influence tumorigenesis.

Conclusions

It is clear that the chromatin context influences replication timing and initiation choices. However, chromatin may additionally play an important role in ensuring replication fidelity and preventing rereplication. Distinct chromatin domains may have increased propensity for rereplication under different circumstances and cell types. This is supported by work in *Drosophila* that demonstrates that heterochromatic regions rereplicate upon loss of geminin (Ding and MacAlpine, 2010). Additionally, some chromatin modifiers such as KMT5A/B/C regulate rereplication on a more global scale (Beck et al., 2012; Tardat et al., 2010). Taken together, these results suggest that proper regulation of chromatin state is critical for suppressing rereplication. Therefore, a "chromatin checkpoint" may be intimately associated with the timing of replication and the propensity to undergo rereplication and copy gain.

Although we have uncovered a single enzyme that can regulate site-specific copy gain, several additional questions remain to be answered (Figure S7M). How does the chromatin environment regulate CNV? Is regulation of methylation of nonhistone substrates involved in modulating copy number (e.g., replication machinery and/or HP1)? Do additional chromatin modifiers regulate CNV and contribute to tumor heterogeneity? What events could promote transient copy gains to be inherited? Future studies that identify additional factors and/or stimuli that address these questions will allow for a more complete picture surrounding copy number variation, rereplication, genome stability, and cancer to emerge.

EXPERIMENTAL PROCEDURES

Extended Experimental Procedures are included in the Supplemental Information.

Cell Culture

Generation of stable cell lines, constructs, and antibodies used can be found in the Extended Experimental Procedures. Transient H3.3 variant RPE cells were transduced with lentiviral stocks provided from the Allis lab in the presence of 8 μg/ml polybrene for 8 hr (Lewis et al., 2013).

Subcellular Localization and Catalytic Activity of KDM4A Deletion Fragments

H3K36me3 and subcellular localization were assayed by examining transfected cells (positive for HA staining; HA.11 Covance) following fixation in 3.7% PFA in PBS (Whetstine et al., 2006).

Immunoprecipitation and Chromatin Immunoprecipitation

HaloTag-purified KDM4A complexes were analyzed and processed by MS Bioworks (Ann Arbor, Michigan), with details in the Extended Experimental Procedures. Immunoprecipitations (IP) were performed essentially as described in Van Rechem et al. (2011).

Chromatin IPs were performed as in Black et al. (2010) with some minor changes. Sonication was performed using a Qsonica Q800R system with a constant chiller. RPE cells were arrested in 2 mM HU for 20 hr prior to crosslinking to assess enrichment in KDM4A, HP1γ, H3K9me3, H3K36me3, and DNA polymerase α at G1/S transition. Data presented are averages from the two independently prepared polyclonal RPE cell lines from at least two independent chromatin preparations per cell line.

Fluorescent In Situ Hybridization

Fluorescent in situ hybridization (FISH) was performed as described in Manning et al. (2010). Probes for 1q12h, 1q telomere, 6p21/chr 14 IGH translocation, and chromosomes 2, 6, 8, and X alpha satellite were purchased from Rainbow Scientific. Probes for 1q12/21.1 (RP11-17L12), Xq13.2 (RP11-451A22), and Xq13.1 (RP11-177A4) were purchased as BAC clones from Children's Hospital Oakland Research Institute (CHORI BacPac) FISH verified clone repository. Probes for 1q21.2 (*BCL9*) and 1q23.3 were purchased from Agilent (SureFISH). For RPE cells, copy gain was scored as any cell with three or more distinct foci. For 293T cells, copy gain was scored for any cell with five or more distinct foci. Comprehensive methods can be found in the Extended Experimental Procedures.

Cesium Chloride Gradient Centrifugation

RPE cells were treated with 100 μM BrdU 14 hr prior to harvest. DNA was purified, digested with RNase A, EcoRI, and BamHI (NEB), and resuspended in TE. 100 μg of DNA was mixed with CsCl in TE (refractive index of 1.4015–1.4031). The CsCl gradient was centrifuged at 44,400 RPM in a VTi-65 rotor for 72 hr at 25°C. Fractions were collected in ~200 μl aliquots, and DNA concentration was measured by Nanodrop. Appropriate fractions were pooled, dialyzed, concentrated, and ethanol precipitated. Each rereplicated pool was diluted to 15 ng/ul stock, and 7.5 ng of rereplicated DNA pool was analyzed by qPCR. Each sample was normalized to its own input prior to determination of fold change in rereplication. Primers used in this study will be provided upon request.

Determination of Cytoband Copy Number and Correlation with KDM4A

Sample-specific mean focal copy numbers for 807 cytobands including X chromosome were annotated by taking an average of GISTIC annotated focal copy numbers for every gene within the same cytoband. The p values for the mean focal copy number changes between *KDM4A* copy-gained samples (GISTIC annotation = +1 or +2) and *KDM4A* copy-neutral samples (GISTIC annotation = 0) across 807 cytobands were annotated by two independent statistical tests (Figures 6A–6C and S6A–S6C; see the Extended Experimental Procedures for details). As positive controls, we also calculated the significance using the gene-specific copy number for *KDM4A* and *KDM4B*. The empirical cumulative distribution functions (the fraction of samples below the given mean focal copy) were determined by enumerating samples having the mean focal copy number less than or equal to the value on the x axis in Figures S6D–S6I for *KDM4A*- and *KDM4B*-amplified (+2), copy-gained (+1), and copy-neutral samples (0). Procedures for RNA-seq and ovarian cancer outcome can be found in the Extended Experimental Procedures.

SUPPLEMENTAL INFORMATION

Supplemental Information includes Extended Experimental Procedures, seven figures, and one table and can be found with this article online at http://dx.doi.org/10.1016/j.cell.2013.06.051.

ACKNOWLEDGMENTS

We are grateful to Ravi Mylvaganam and the MGH Flow Cytometry core for assistance with the cell sorting. We thank Mo Motamedi for helpful comments on the manuscript. This work was supported by funding to J.R.W. from the Ellison Medical Foundation, CA059267 and R01GM097360. G.G. and J.K. are supported by NIH U24CA143845. J.C.B. was a Fellow of The Jane Coffin Childs Memorial Fund for Medical Research. This investigation has been aided by a grant from The Jane Coffin Childs Memorial Fund for Medical Research. N.J.D. is supported by R01CA155202. A.L.M. is supported by MGH ECOR Tosteson Postdoctoral Fellowship. C.M. is supported by CCSG P30CA013330.

Received: March 6, 2013
Revised: May 8, 2013
Accepted: June 28, 2013
Published: July 18, 2013

REFERENCES

Alabert, C., and Groth, A. (2012). Chromatin replication and epigenome maintenance. Nat. Rev. Mol. Cell Biol. *13*, 153–167.

Arias, E.E., and Walter, J.C. (2007). Strength in numbers: preventing rereplication via multiple mechanisms in eukaryotic cells. Genes Dev. *21*, 497–518.

Beck, D.B., Burton, A., Oda, H., Ziegler-Birling, C., Torres-Padilla, M.E., and Reinberg, D. (2012). The role of PR-Set7 in replication licensing depends on Suv4-20h. Genes Dev. *26*, 2580–2589.

Beroukhim, R., Mermel, C.H., Porter, D., Wei, G., Raychaudhuri, S., Donovan, J., Barretina, J., Boehm, J.S., Dobson, J., Urashima, M., et al. (2010). The landscape of somatic copy-number alteration across human cancers. Nature *463*, 899–905.

Berry, W.L., Shin, S., Lightfoot, S.A., and Janknecht, R. (2012). Oncogenic features of the JMJD2A histone demethylase in breast cancer. Int. J. Oncol. *41*, 1701–1706.

Black, J.C., Allen, A., Van Rechem, C., Forbes, E., Longworth, M., Tschöp, K., Rinehart, C., Quiton, J., Walsh, R., Smallwood, A., et al. (2010). Conserved antagonism between JMJD2A/KDM4A and HP1γ during cell cycle progression. Mol. Cell *40*, 736–748.

Brunet, A., Armengol, L., Heine, D., Rosell, J., García-Aragonés, M., Gabau, E., Estivill, X., and Guitart, M. (2009). BAC array CGH in patients with Velocardiofacial syndrome-like features reveals genomic aberrations on chromosome region 1q21.1. BMC Med. Genet. *10*, 144.

Brzustowicz, L.M., Hodgkinson, K.A., Chow, E.W., Honer, W.G., and Bassett, A.S. (2000). Location of a major susceptibility locus for familial schizophrenia on chromosome 1q21-q22. Science *288*, 678–682.

Davidson, I.F., Li, A., and Blow, J.J. (2006). Deregulated replication licensing causes DNA fragmentation consistent with head-to-tail fork collision. Mol. Cell *24*, 433–443.

Ding, Q., and MacAlpine, D.M. (2010). Preferential re-replication of Drosophila heterochromatin in the absence of geminin. PLoS Genet. *6*, e1001112.

Hanahan, D., and Weinberg, R.A. (2011). Hallmarks of cancer: the next generation. Cell *144*, 646–674.

Hastings, P.J., Lupski, J.R., Rosenberg, S.M., and Ira, G. (2009). Mechanisms of change in gene copy number. Nat. Rev. Genet. *10*, 551–564.

Hook, S.S., Lin, J.J., and Dutta, A. (2007). Mechanisms to control rereplication and implications for cancer. Curr. Opin. Cell Biol. *19*, 663–671.

Inoue, J., Otsuki, T., Hirasawa, A., Imoto, I., Matsuo, Y., Shimizu, S., Taniwaki, M., and Inazawa, J. (2004). Overexpression of PDZK1 within the 1q12-q22 amplicon is likely to be associated with drug-resistance phenotype in multiple myeloma. Am. J. Pathol. *165*, 71–81.

Jiang, X.R., Jimenez, G., Chang, E., Frolkis, M., Kusler, B., Sage, M., Beeche, M., Bodnar, A.G., Wahl, G.M., Tlsty, T.D., and Chiu, C.P. (1999). Telomerase expression in human somatic cells does not induce changes associated with a transformed phenotype. Nat. Genet. *21*, 111–114.

Kiang, L., Heichinger, C., Watt, S., Bähler, J., and Nurse, P. (2010). Specific replication origins promote DNA amplification in fission yeast. J. Cell Sci. *123*, 3047–3051.

Kim, T.D., Shin, S., Berry, W.L., Oh, S., and Janknecht, R. (2012). The JMJD2A demethylase regulates apoptosis and proliferation in colon cancer cells. J. Cell. Biochem. *113*, 1368–1376.

Kracikova, M., Akiri, G., George, A., Sachidanandam, R., and Aaronson, S.A. (2013). A threshold mechanism mediates p53 cell fate decision between growth arrest and apoptosis. Cell Death Differ. *20*, 576–588.

Kudoh, K., Takano, M., Koshikawa, T., Hirai, M., Yoshida, S., Mano, Y., Yamamoto, K., Ishii, K., Kita, T., Kikuchi, Y., et al. (1999). Gains of 1q21-q22 and 13q12-q14 are potential indicators for resistance to cisplatin-based chemotherapy in ovarian cancer patients. Clin. Cancer Res. *5*, 2526–2531.

Kuo, A.J., Song, J., Cheung, P., Ishibe-Murakami, S., Yamazoe, S., Chen, J.K., Patel, D.J., and Gozani, O. (2012). The BAH domain of ORC1 links H4K20me2 to DNA replication licensing and Meier-Gorlin syndrome. Nature *484*, 115–119.

Lewis, P.W., Muller, M.M., Koletsky, M.S., Cordero, F., Lin, S., Banaszynski, L.A., Garcia, B.A., Muir, T.W., Becher, O.J., and Allis, C.D. (2013). Inhibition of PRC2 activity by a gain-of-function H3 mutation found in pediatric glioblastoma. Science *340*, 857–861.

Luo, J., Solimini, N.L., and Elledge, S.J. (2009). Principles of cancer therapy: oncogene and non-oncogene addiction. Cell *136*, 823–837.

Mallette, F.A., and Richard, S. (2012). JMJD2A promotes cellular transformation by blocking cellular senescence through transcriptional repression of the tumor suppressor CHD5. Cell Rep. *2*, 1233–1243.

Mallette, F.A., Mattiroli, F., Cui, G., Young, L.C., Hendzel, M.J., Mer, G., Sixma, T.K., and Richard, S. (2012). RNF8- and RNF168-dependent degradation of KDM4A/JMJD2A triggers 53BP1 recruitment to DNA damage sites. EMBO J. *31*, 1865–1878.

Manning, A.L., Longworth, M.S., and Dyson, N.J. (2010). Loss of pRB causes centromere dysfunction and chromosomal instability. Genes Dev. *24*, 1364–1376.

Maslov, A.Y., and Vijg, J. (2009). Genome instability, cancer and aging. Biochim. Biophys. Acta *1790*, 963–969.

Mermel, C.H., Schumacher, S.E., Hill, B., Meyerson, M.L., Beroukhim, R., and Getz, G. (2011). GISTIC2.0 facilitates sensitive and confident localization of the targets of focal somatic copy-number alteration in human cancers. Genome Biol. *12*, R41.

Negrini, S., Gorgoulis, V.G., and Halazonetis, T.D. (2010). Genomic instability—an evolving hallmark of cancer. Nat. Rev. Mol. Cell Biol. *11*, 220–228.

Papamichos-Chronakis, M., and Peterson, C.L. (2013). Chromatin and the genome integrity network. Nat. Rev. Genet. *14*, 62–75.

Schimke, R.T. (1984). Gene amplification, drug resistance, and cancer. Cancer Res. *44*, 1735–1742.

Snaith, H.A., and Forsburg, S.L. (1999). Rereplication phenomenon in fission yeast requires MCM proteins and other S phase genes. Genetics *152*, 839–851.

Stratton, M.R., Campbell, P.J., and Futreal, P.A. (2009). The cancer genome. Nature *458*, 719–724.

Takano, M., Kudo, K., Goto, T., Yamamoto, K., Kita, T., and Kikuchi, Y. (2001). Analyses by comparative genomic hybridization of genes relating with cisplatin-resistance in ovarian cancer. Hum. Cell *14*, 267–271.

Tardat, M., Brustel, J., Kirsh, O., Lefevbre, C., Callanan, M., Sardet, C., and Julien, E. (2010). The histone H4 Lys 20 methyltransferase PR-Set7 regulates replication origins in mammalian cells. Nat. Cell Biol. *12*, 1086–1093.

Van Rechem, C., Black, J.C., Abbas, T., Allen, A., Rinehart, C.A., Yuan, G.C., Dutta, A., and Whetstine, J.R. (2011). The SKP1-Cul1-F-box and leucine-rich repeat protein 4 (SCF-FbxL4) ubiquitin ligase regulates lysine demethylase 4A (KDM4A)/Jumonji domain-containing 2A (JMJD2A) protein. J. Biol. Chem. *286*, 30462–30470.

Vassilev, L.T. (2006). Cell cycle synchronization at the G2/M phase border by reversible inhibition of CDK1. Cell Cycle *5*, 2555–2556.

Whetstine, J.R., Nottke, A., Lan, F., Huarte, M., Smolikov, S., Chen, Z., Spooner, E., Li, E., Zhang, G., Colaiacovo, M., and Shi, Y. (2006). Reversal of histone lysine trimethylation by the JMJD2 family of histone demethylases. Cell *125*, 467–481.

Wong, N., Lam, W.C., Lai, P.B., Pang, E., Lau, W.Y., and Johnson, P.J. (2001). Hypomethylation of chromosome 1 heterochromatin DNA correlates with q-arm copy gain in human hepatocellular carcinoma. Am. J. Pathol. *159*, 465–471.

Yakut, T., Schulten, H.J., Demir, A., Frank, D., Danner, B., Egeli, U., Gebitekin, C., Kahler, E., Gunawan, B., Urer, N., et al. (2006). Assessment of molecular events in squamous and non-squamous cell lung carcinoma. Lung Cancer *54*, 293–301.

Cell

EXTENDED EXPERIMENTAL PROCEDURES

Cell Culture

HEK293T (called 293T throughout) and hTERT-RPE-1 (called RPE throughout) cells were maintained in DMEM with 10% fetal bovine serum, 1% penicillin/streptomycin, and L-glutamine. Stable 293T cell lines were generated as in (Black et al., 2010). Stable RPE cell lines were generated by retroviral transduction of MSCV-GFP or MSCV-GFP-KDM4A. Cells were selected for 96 hr with puromycin. All experiments on stable cells were performed after two months of culture post infection with KDM4A. Transient transfection experiments were performed using Roche X-tremeGENE 9 DNA transfection reagent in OPTI-MEM I media (GIBCO) for four hours. Media was then replaced with standard DMEM. For concomitant overexpression and depletion in 293T cells, shRNA was transfected for 4 hr, cells recovered in DMEM for 20 hr and cells were transfected a second time with additional shRNA and KDM4A expression plasmid. Cells were harvested for FISH 48 hr following the second transfection. No selection was used in transient transfection experiments.

Expression Plasmids

The pFN21A clone expressing an N-Terminal HaloTag fusion of human full-length KDM4A or Suv39h1 (NM_014663) was obtained from Kazusa DNA Research Institute (Kisarazu, Japan). HaloTag (ADN27525.1) control vector (Promega) was used for expression of the HaloTag protein alone. MSCV-GFP-KDM4A, MSCV-GFP-H188A, MSCV-RFP-HP1, pSuper and pSuper sh2A.1 constructs were made as described (Black et al., 2010). N-terminal HA-FLAG (NHF) deletion constructs were generated using primers at the indicated amino acid residues and cloned into pEntry using Gateway technology (Invitrogen). Fragments were transferred to N-terminal HA-FLAG (NHF) destination vector following the manufacturer's instructions. H188A contains two point mutations to eliminate catalytic activity H188A and W208R (Black et al., 2010). All clones were sequence verified.

Western Blots

Western blots were performed as in (Black et al., 2010). Antibodies used were: KDM4A (Neuro mAB, 75-189), β-actin (Millipore), GFP (Neuro mAB, 73-131), RFP (Abcam, ab62341), p53 (Santa Cruz, sc-126), MCM2 (Cell Signaling, #3619S), MCM3 (Cell Signaling, #4012S), MCM7 (Cell Signaling, #3735S), Halo (Promega), Actinin (Santa Cruz, sc-17829), HA 12CA5 (Roche), FLAG M2 (Sigma), DNA Pol α (Abcam, ab31777).

G-Band and Spectral Karyotyping

G-Band analysis was performed and analyzed by WiCell Cytogenetics Institute (Wisconsin). SKY and corresponding analysis was performed by Cristina Montagna in the Molecular Cytogenetic Core at Albert Einstein College of Medicine. The RPE stable cell lines were analyzed by SKY two independent times: once after six months in culture and a second time after an additional three months of culture.

Subcellular Localization and Catalytic Activity of KDM4A Deletion Fragments

The indicated NHF-tagged KDM4A deletion constructs were transfected into RPE cells grown on coverslips in 10 cm dishes using X-tremeGENE 9 DNA transfection reagent (Roche). H3K36me3 and subcellular localization were assayed by examining transfected cells (positive for HA staining; HA.11 Covance) following fixation in 3.7% PFA in PBS (Whetstine et al., 2006).

Immunoprecipitation and Chromatin Immunoprecipitation

Immunoprecipitations were performed essentially as described in (Van Rechem et al., 2011). Briefly, cells were lysed in cellular lysis buffer (5mM PIPES, 85mM KCl, 0.5% NP40) and nuclei were collected following centrifugation. Nuclei were lysed in IPH buffer with sonication, lysates were cleared and immunoprecipitations were performed in the presence of 100ug/ml ethidium bromide and digested with 0.25ul benzonase to eliminate protein-nucleic acid interactions. Immunoprecipitation from 293T cells were carried out in IPH with 150mM NaCl and from RPE cells in 300mM NaCl. Immunoprecipitation of HaloTag polymerase subunits with endogenous KDM4A was performed according to the manufacturers protocol (Promega) with minor modification. Whole cell lysates were prepared using sonication of cells in Halo lysis buffer. Immunoprecipitations were performed with ethidium bromide overnight at 4þC. Elution was performed using SDS sample loading buffer.

Chromatin immunoprecipitations were performed as in (Black et al., 2010) with some minor changes. Sonication was performed using a Qsonica Q800R system with a constant chiller. For ChIP, RPE cells were arrested in 2mM HU for 20 hr prior to crosslinking to assess enrichment in KDM4A, HP1γ, H3K9me3, H3K36me3, and DNA polymerase α at G1/S transition. For release from HU (as indicated in figures), HU containing media was removed by aspiration, and cells were rinsed twice with fresh DMEM prior to addition of fresh DMEM for release for the indicated times. 1 to 10ug of chromatin was used for each IP, which was dependent on the antibody used. For HP1γ, chromatin was prepared and sonicated in TE with 1%SDS, diluted to 0.2% SDS prior to dilution for the immunoprecipitation. Chromatin for histone ChIP was prepared and sonicated in TE with 1% SDS. Chromatin for KDM4A, Polα, and MCM7 was prepared and sonicated in TE with 0.2% SDS. Prior to ChIP, RPE chromatin was precleared for one hour with protein A agarose, and for one hour with magnetic protein A or G beads (Invitrogen; to match antibody type). Immunoprecipitated DNA was purified using either PCR Purification Columns (Promega) or AMPureXP. Data presented are averages from the two

independently prepared polyclonal RPE cell lines from at least two independent chromatin preparations per cell line. Antibodies used for ChIP are as follows: DNA Polα (Abcam, ab31777 lot 290601), MCM7 (Cell Signaling, #3735S lots 02/2013 and 03/2013), KDM4A (Black et al., 2010), HP1γ (Millipore, 05-690 lot DAM1501782), H3K9me3 (Abcam, ab8898 lot GR30928-1), H3K36me3 (Abcam, ab9050 lot GR10860-1), H3 (Abcam, ab1791 lot GR63387-1).

KDM4A Cytogentic Band Enrichment

KDM4A ChIP-chip on chromosome 1–4 was reported previously (Van Rechem et al., 2011). Raw data was re-analyzed as follows. ChIP signals were log-transformed (base 2) and normalized by using quantile normalization then averaged over replicates. Input signals were also quantile normalized and the results were subtracted from the normalized ChIP signals, and the results were referred to as log-ratio. Cytogenetic band locations were downloaded from UCSC Genome Browser using HG18. The probe-level log-ratio values were averaged over each cytogenetic band and then each cytogenetic band was transformed to z-scores. Raw data are deposited under GSE48765.

Fluorescent In Situ Hybridization

Fluorescent in situ hybridization (FISH) was performed as described in (Manning et al., 2010). Probes for 1q12h, 1q telomere, 6p21/chr14 IGH translocation and chromosome 2, 6, 8, and X alpha satellite were purchased from Rainbow Scientific. Probes for 1q12/21.1 (RP11-17L12), Xq13.2 (RP11-451A22), Xq13.1 (RP11-177A4) were purchased as BAC clones from Children's Hospital Oakland Research Institute (CHORI BacPac) FISH verified clone repository. Oligonucleotide probes for 1q21.2 (BCL9) and 1q23.3 were purchased from Agilent (SureFISH). BACS were prepared utilizing PureLink HiPure Plasmid Filter Maxiprep kit (Life Technologies) using the recommended modified wash buffer. Probes were nick translated (Abbot Molecular Kit) in the presence of fluorescently labeled dTTP (Enzo Life Science). Images of multiple planes of fields of nuclei were acquired on an Olympus IX81 Spinning Disk Microscope and analyzed using Slidebook 5.0 software. We used a conservative scoring metric for copy gain. Any foci that were touching were scored as a single foci to prevent increased numbers due to normally replicated foci. For RPE cells, copy gain was scored as any cell with 3 or more distinct foci. For 293T cells, copy gain was scored for any cell with 5 or more distinct foci. For RPE cells each experiment includes at least one replicate from the two different polyclonal stable cell preparations. At least 100 cells for each replicate were scored for all experiments except analysis of single cell clones.

Infection with Histone H3.3 Variants

Lentiviral stocks provided from the Allis lab were used to infect RPE cells in the presence of 8 μg/ml polybrene for 8 hr (Lewis et al., 2013). Cells were washed 2 times with DMEM. Cells were collected 24 hr later for analysis by FISH and Western blot. Incorporation of histone variants was confirmed by subcellular fractionation and Western blotting.

Fluorescent In Situ Hybridization Coupled to Chromosome 1 Paint

FISH/Paint was performed using the 1q12/21 probe labeled in Spectrum Orange combined with a chromosome 1 painting probe labeled in Spectrum Green. The chromosome paint probe was generated using standard protocols (Montagna et al., 2002). Equal volumes of locus specific and paint probe resuspended in hybridization solution (50% dextran sulfate/2 × SSC) were combined and denatured at 85°C for 5 min, applied to the slides and incubated overnight at 37°C in a humidified chamber. Before hybridization the slides with interphase nuclei were denatured with 50% formamide/2 × SSC at 80°C for 1.5 min and then dehydrated with serial ethanol washing steps (ice cold 70%, 90% and 100% for 3 min each). After hybridization the slides were washed three times for 5 min with 50% formamide/2 × SSC, 1 × SSC and 4 × SSC/0.1%Tween. Slides were dehydrated with serial ethanol washing steps (as above) and mounted with ProLong Gold antifade reagent with DAPI (Invitrogen) for imaging. FISH/Paint images were acquired with a manual inverted fluorescence microscope (Axiovert 200, Zeiss) with fine focusing oil immersion lens (× 40, NA 1.3 oil and × 60, NA 1.35 oil). Multiple focal planes were acquired for each channel to ensure that signals on different focal planes were included. The resulting fluorescence emissions were collected using 425–475 nm (for DAPI), 546–600 nm (for spectrum orange), and 500–550 nm (for AlexaFluor488) filters. The microscope was equipped with a Camera Hall 100 and the Applied Spectral Imaging software.

Cesium Chloride Gradient Centrifugation

RPE cells were treated with 100 μM BrdU 14 hr prior to harvest. Cells were lysed in RIPA supplemented with 100μg of RNase A (Fisher) for 2 hr at 37°C. Buffer was supplemented to 1% SDS and 20 μg of proteinase K was added and digested overnight at 55°C. DNA was extracted three times with phenol:chloroform:isoamyl alcohol and ethanol precipitated. Precipitated DNA (approximately 300 μg) was resuspended in NEB buffer 2 supplemented with RNase A and digested with 200U of EcoRI and BamHI (NEB) overnight at 37°C. Digests were supplemented to 1% SDS and digested with 10 μg of proteinase K for 1 hr at 55°C. DNA was extracted with phenol:chloroform:isoamyl alcohol and ethanol precipitated. Precipitated DNA was resuspended in TE and concentration determined by Nanodrop. 100 μg of DNA was mixed with 1g/ml CsCl in TE (refractive index of 1.4015-1.4031) in Quick-Seal ultracentrifuge tubes (Beckman). The CsCl gradient was centrifuged at 44,400 RPM in a VTi-65 rotor for 72 hr at 25°C. Fractions were collected from the bottom of the gradient in ~200 μl aliquots. DNA concentration of each fraction was measured by Nanodrop. Appropriate fractions were pooled, dialyzed against 0.1X TE and concentrated by dialysis against 0.1XTE with 40% glycerol. Concentrated pools were ethanol precipitated and resuspended in ddH2O prior to analysis by quantitative PCR (qPCR). Each

re-replicated fraction was diluted to 15ng/ul stock and 7.5ng of re-replicated DNA pool was analyzed by qPCR on a Roche LC480 using FastStart Universal SYBR Green Master Mix (Roche) following the manufacturer's instructions. 7.5ng of input DNA was analyzed by qPCR at the same time. Each sample was normalized to its own input prior to determination of fold-change in re-replication. Primers used in this study will be provided upon request.

HaloTag Mammalian Pull-Down Assay for Mass Spectrometry

HEK293T cells (12×10^6 cells) were plated in a 150 mm dish and grown to 70%–80% confluence (approximately 18 hr). The cells were then transfected with 30μg of plasmid DNA using FuGENE HD Transfection Reagent (Promega) for 24 hr, according to manufacturer's protocol. Cells expressing Halo-KDM4A or Halo-CTRL were incubated in mammalian lysis buffer (50mM Tris-HCl, pH 7.5, 150mM NaCl, 1% Triton X-100, and 0.1% sodium deoxycholate) supplemented with Protease Inhibitor cocktail (Promega) and RQ1 RNase-Free DNase (Promega) for 10 min on ice. Lysate was then homogenized with a syringe and centrifuged at 14.000 x g for 5 min to pellet cellular debris. Clarified lysate was incubated with HaloLink Resin (Promega) that had been pre-equilibrated in resin wash buffer (TBS and 0.05% IGEPAL CA-640 [Sigma]) for 15 min at 22°C with rotation. Resin was then washed 5 times with wash buffer, and protein interactors were eluted with SDS elution buffer (50mM Tris-HCl, pH 7.5, and 1% SDS).

Mass Spectrometry Analysis

HaloTag pulldown purified complexes were analyzed and processed by MS Bioworks, LLC (Ann Arbor, Michigan). The samples were separated on a SDS-PAGE gel, which was then Coomassie stained and cut into 10 fragments. Each gel piece was processed with the Progest Protein Digestion Station (Digilab). Briefly, gel slices were washed using 25 mM ammonium bicarbonate and acetonitrile, followed by reduction with 10 mM dithiothreitol, and alkylation with 50 mM iodoacetamide. Proteins were digested with trypsin (Promega) for 4 hr and digestion was quenched with formic acid. Gel digests were analyzed directly by nano LC/MS/MS with a NanoAcquity HPLC (Waters) interfaced with an Orbitrap Velos Pro (Thermo Scientific) tandem mass spectrometer. Digested peptides were loaded on a trapping column and eluted over a 75 μm analytical column packed with Jupiter Proteo Resin (Phenomenex) at 350nl/min. The mass spectrometer was operated in data-dependent mode, with MS performed in the Orbitrap at 60.000 full width at half maximum (FWHM) resolution, and MS/MS performed in the LTQ. The 15 most abundant ions were selected for MS/MS. The data were searched with Mascot (Matrix Science) against the concatenated forward/decoy UniProt Human Database, and Mascot DAT files were visualized and filtered by Scaffold (Proteome Software). Data were filtered using a minimum protein value of 90%, a minimum peptide value of 50% (Protein and Peptide Prophet scores), and required at least two unique peptides per protein. Spectral counting was performed and normalized spectral abundance factors determined. Data were reported at less than 1% false discovery rate (FDR) at the protein level based on counting the number of forward and decoy matches. Interacting proteins were analyzed using IPA for pathway analysis (Ingenuity Systems).

Flow Cytometry Analysis of Cell Cycle and Apoptosis

Asynchronously growing, or G1/S or G2 arrested cells were prepared and fixed as in (Black et al., 2010). Cell cycle was analyzed by PI staining and analyzed using a BD FACS ARIA II. Apoptosis was determined using Annexin V and PI staining following the manufacturer's instructions (Life Technologies).

KDM4A Copy Number Determination in TCGA Data Set

The somatic copy number alterations (SCNAs) for 24,176 genes of the pan-cancer data set including 4,420 samples across multiple tumor types are annotated by GISTIC2.0 (Beroukhim et al., 2007; Beroukhim et al., 2010; Network, 2008). The copy number change in each gene is defined as possessing deep deletion (−2), shallow deletions (−1), neutral copy number (0), low gain (+1), and high gain (+2) in each sample using sample-specific thresholds. High gains are segments with copy number that exceed the maximum median chromosomal arm copy number for that sample by at least 0.1; low gains are segments with copy numbers from 2.1 to the high gain threshold; neutral segments have copy numbers between 1.9 and 2.1; shallow losses have copy numbers between 1.9 and the deep deletion threshold; and deep deletion have copy numbers that are below the minimum median chromosomal arm copy number for that sample by at least 0.1.

KDM4A mRNA expression from RNA-Seq in TCGA Data Set

Reads per kilobase of exon model per million mapped reads (RPKM) were annotated for 16,407 genes in 1,953 samples across multiple tumor types. 1770 samples having both copy number and RPKM data were used to quantify an association between copy number alterations and the mRNA expression levels in KDM4A in Figure 1B and 1D, and Figure S1. The "Gain" group corresponds to the sample set with *KDM4A* GISTIC annotation = +1 or +2, the "No change" group corresponds to the samples set with *KDM4A* GISTIC annotation = 0, and the "Loss" group is associated to the sample set with *KDM4A* GISTIC annotation = −1 or −2.

Clinical Data in TCGA Data Set

Overall survival in 541 Ovarian Cancer samples (256 alive and 285 deceased) was defined as the interval from the date of initial surgical resection to the date of last known contact or death. The association of the *KDM4A* copy number status, Del (−2), Loss (−1),

None (0), Gain (+1), Amp (+2) to the clinical outcome in Figure 1E through 1H was tested for 285 deceased patients by Student's t test (one-tailed) and statistical significance was considered when $p < 0.05$.

Determination of Cytoband Copy Number and Correlation with KDM4A in TCGA Data Set

In addition to the copy number annotation for each gene, the mean focal copy number for 807 cytobands including X chromosome were annotated in each sample by taking an average of focal copy numbers of every genes within the same cytoband. Arm-level SCNA contributions to the mean focal copy number in each cytoband were removed by only considering GISTIC annotated focal copy numbers much smaller than a chromosome arm or entire chromosome. Detecting chromosomal regions significantly co-amplified with *KDM4A* copy gains or amplifications was first performed by the one-tailed Student's t test for the mean focal copy number changes between *KDM4A* copy-gained samples (GISTIC annotation = +1 or +2) and *KDM4A* copy-neutral samples (GISTIC annotation = 0) across 807 cytobands. We also calculated the significance using the gene-specific copy-number for *KDM4A* and *KDM4B* as positive controls (Figure 6A-C). We also performed the second independent test (Figure S6A-S6C) by approximating a null distribution of mean cytoband copy differences by a normal function $N(\mu_{12} - \mu_0, \sigma_0^2/n_0 + \sigma_{12}^2/n_{12})$ where μ_0 and μ_{12} are samples means across all cytobands, σ_0^2 and σ_{12}^2 are mean sample-specific variances within each group, and n_0 and n_{12} are the number of samples in *KDM4A* copy-neutral and *KDM4A* copy-gained groups, respectively. This test is based on comparing the means of the two sets while permuting values within each of the samples (and using a Gaussian approximation). The p-values across 807 cytobands were annotated by computing the probability of more extreme differences than the corresponding cytoband copy difference in the null distribution. The empirical cumulative distribution functions (the fraction of samples below the given mean focal copy) were determined by enumerating samples having the mean focal copy number less than or equal to the value on the *x* axis in Figure S6D-S6I for *KDM4A* and *KDM4B* amplified (+2), copy-gained (+1), and copy-neutral samples (0).

SUPPLEMENTAL REFERENCES

Beroukhim, R., Getz, G., Nghiemphu, L., Barretina, J., Hsueh, T., Linhart, D., Vivanco, I., Lee, J.C., Huang, J.H., Alexander, S., et al. (2007). Assessing the significance of chromosomal aberrations in cancer: methodology and application to glioma. Proc. Natl. Acad. Sci. USA *104*, 20007–20012.

Montagna, C., Andrechek, E.R., Padilla-Nash, H., Muller, W.J., and Ried, T. (2002). Centrosome abnormalities, recurring deletions of chromosome 4, and genomic amplification of HER2/neu define mouse mammary gland adenocarcinomas induced by mutant HER2/neu. Oncogene *21*, 890–898.

Network, C.G.A.R.; Cancer Genome Atlas Research Network. (2008). Comprehensive genomic characterization defines human glioblastoma genes and core pathways. Nature *455*, 1061–1068.

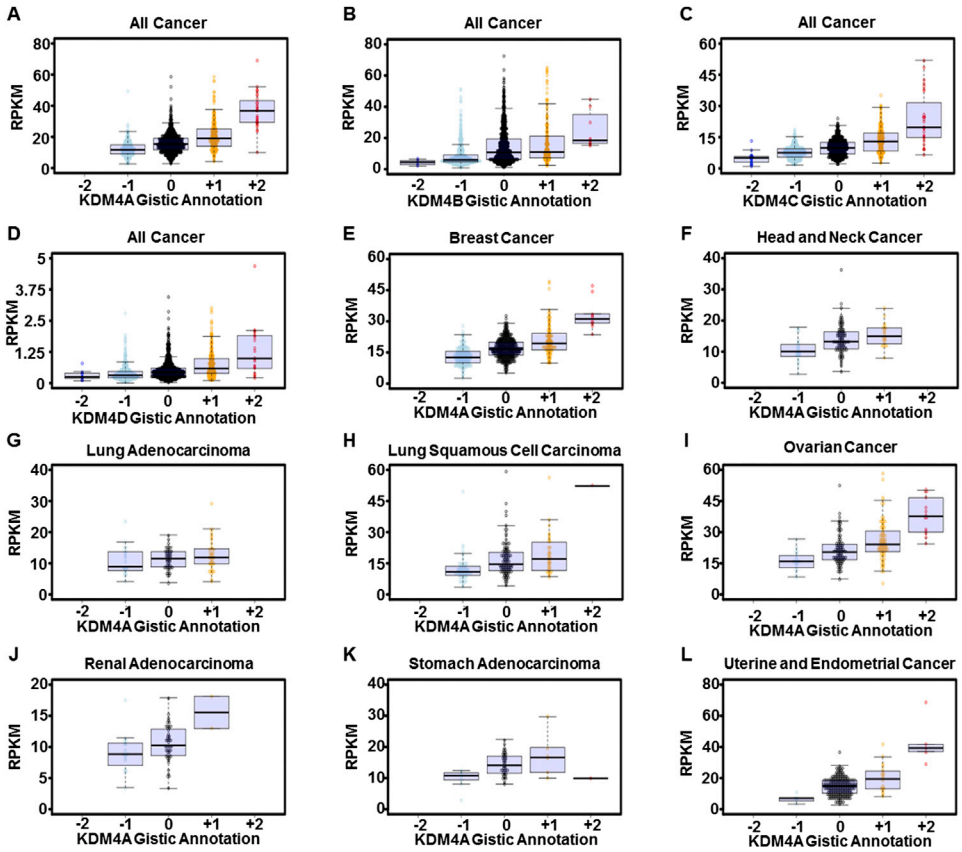

Figure S1. Amplification and Overexpression of KDM4A in Cancer, Related to Figure 1

(A) Analysis of RNaseq data from all cancer types indicating expression level of *KDM4A* relative to *KDM4A* copy number binned by GISTIC annotation.
(B) Analysis of RNaseq data from all cancer types indicating expression level of *KDM4B* relative to *KDM4B* copy number binned by GISTIC annotation.
(C) Analysis of RNaseq data from all cancer types indicating expression level of *KDM4C* relative to *KDM4C* copy number binned by GISTIC annotation.
(D) Analysis of RNaseq data from all cancer types indicating expression level of *KDM4D* relative to *KDM4D* copy number binned by GISTIC annotation.
(E) Analysis of RNaseq data from Breast Cancer indicating expression level of *KDM4A* relative to *KDM4A* copy number binned by GISTIC annotation.
(F) Analysis of RNaseq data from Head and Neck squamous cell carcinoma indicating expression level of *KDM4A* relative to *KDM4A* copy number binned by GISTIC annotation.
(G) Analysis of RNaseq data from lung adenocarcinoma indicating expression level of *KDM4A* relative to *KDM4A* copy number binned by GISTIC annotation.
(H) Analysis of RNaseq data from lung squamous cell carcinoma indicating expression level of *KDM4A* relative to *KDM4A* copy number binned by GISTIC annotation.
(I) Analysis of RNaseq data from ovarian cancer indicating expression level of *KDM4A* relative to *KDM4A* copy number binned by GISTIC annotation.
(J) Analysis of RNaseq data from renal adenocarcinoma indicating expression level of *KDM4A* relative to *KDM4A* copy number binned by GISTIC annotation.
(K) Analysis of RNaseq data from stomach adenocarcinoma indicating expression level of *KDM4A* relative to *KDM4A* copy number binned by GISTIC annotation.
(L) Analysis of RNaseq data from uterine and endometrial cancer indicating expression level of *KDM4A* relative to *KDM4A* copy number binned by GISTIC annotation.

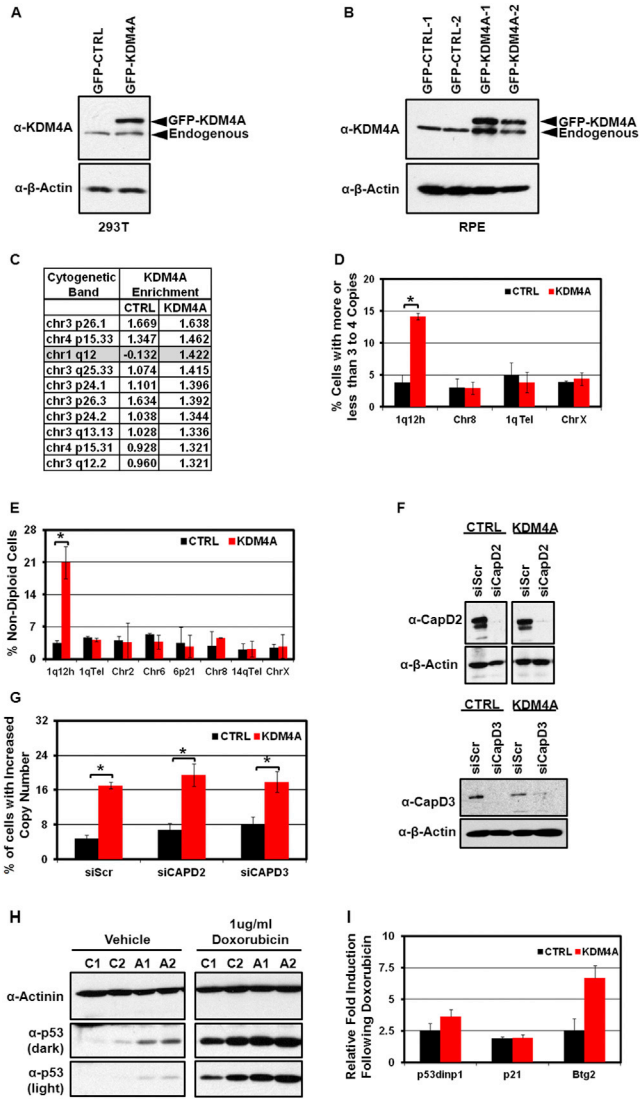

Figure S2. Enrichment of KDM4A in a Specific Cytogenetic Band that Has Altered Copy Number, Related to Figure 2

(A) Western blot depicting expression of GFP-KDM4A in a stable 293T cell line.

(B) Western blot depicting expression of GFP-KDM4A in two different polyclonal stable RPE cells.

(C) Table depicting increased binding of KDM4A in chr1 q12 cytogenetic band in 293T cells overexpressing KDM4A. Enrichment in ChIP-chip data is depicted as the Z-score for the average KDM4A/Input level for each probe in the cytogenetic band.

(D) FISH analysis of 293T cells stably overexpressing GFP-CTRL or GFP-KDM4A. Data are presented as percent of cells with foci number different from the mean (not 3 or 4 foci in 293T cells).

(E) FISH analysis of RPE cells stably overexpressing GFP-CTRL or GFP-KDM4A. Data are presented as percent of cells with foci number different from the mean (not 2 foci in RPE cells).

(F) Western blot demonstrating siRNA depletion of CapD2 and CapD3 in CTRL and KDM4A cells. GFP-CTRL and GFP-KDM4A panels for CapD2 are the same exposure from a different, non-adjacent section of the same Western blot.

(G) FISH analysis for 1q12h in RPE cells stably overexpressing GFP-CTRL or GFP-KDM4A treated with siRNA against condensin 1 (CAPD2) and condensing 2 (CAPD3).

(H) Western analysis of p53 induction following DNA damage by Doxorubicin (1uM for 16 hr) in GFP-CTRL (C1 and C2) or GFP-KDM4A cells (A1 and A2).

(I) Induction of p53 target genes analyzed by quantitative PCR after reverse transcription from doxorubicin damaged GFP-CTRL or GFP-KDM4A cells. Data are presented as fold induction relative to its own uninduced stable cell and normalized to expression of β-actin. Error bars represent the SEM. Asterisk indicates $p < 0.05$ for comparison indicated by bracket using two-tailed students t test.

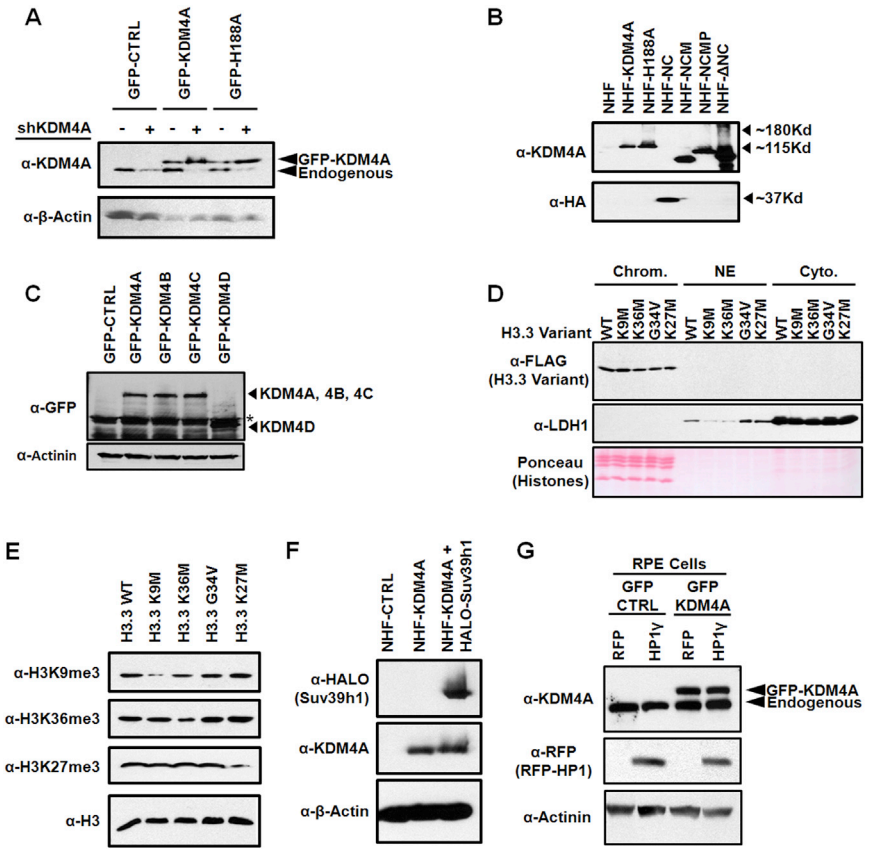

Figure S3. Verification of KDM4A Expression and H3.3 Incorporation, Related to Figure 3

(A) Expression of KDM4A following depletion and overexpression of GFP-CTRL or GFP-KDM4A in 293T cells.

(B) Expression of NHF-tagged KDM4A deletion constructs in RPE cells. Since the NC constructs lacks the KDM4A antibody epitope we show the HA Western blot for this fragment.

(C) Expression of GFP-KDM4A, GFP-KDM4B, GFP-KDM4C, and GFP-KDM4D in transiently transfected RPE cells. * indicates a non-specific band.

(D) Expression and incorporation into chromatin of FLAG-tagged H3.3 variants.

(E) Expression of HA-FLAG-tagged H3.3 K-to-M variants reduced the corresponding tri-methylation.

(F) Expression of KDM4A and Halo-Suv39h1 in transiently transfected RPE cells.

(G) Expression of KDM4A and RFP-HP1γ in transiently transfected RPE cells. Panels were assembled from the same exposure from non-adjacent lanes on different sections of the same blot.

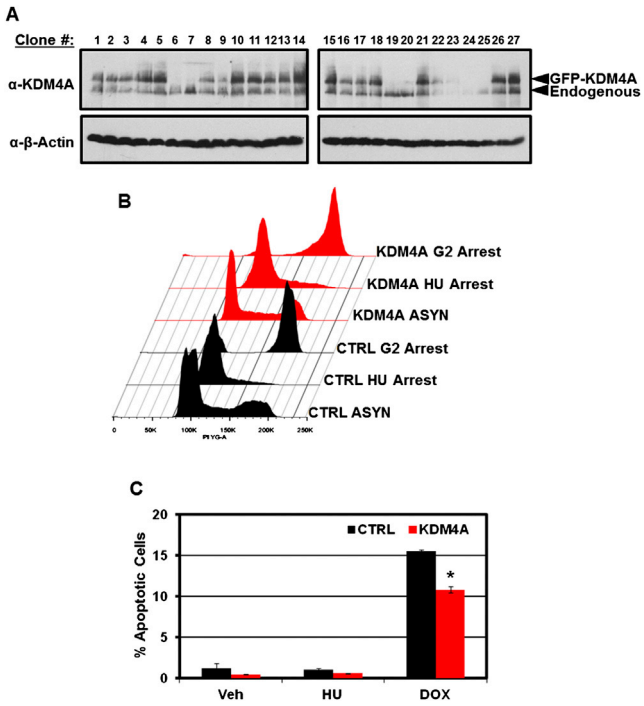

Figure S4. Verification of KDM4A Expression, Cell-Cycle Profile, and Apoptosis

(A) Expression of KDM4A and GFP-KDM4A in RPE stable clones.

(B) FACS analysis demonstrating HU and G2 arrest of CTRL and KDM4A RPE stable cells. Total DNA content as measured using propidium iodide is depicted on the *x* axis.

(C) KDM4A overexpressing RPE cells are not more apoptotic following treatment with hydroxyurea (HU) as measured by percent Annexin V positive cells. However, 12 hr of doxorubicin treatment induces apoptosis. Asterisk indicates $p < 0.05$ compated to CTRL + DOX using two-tailed Student's t test.

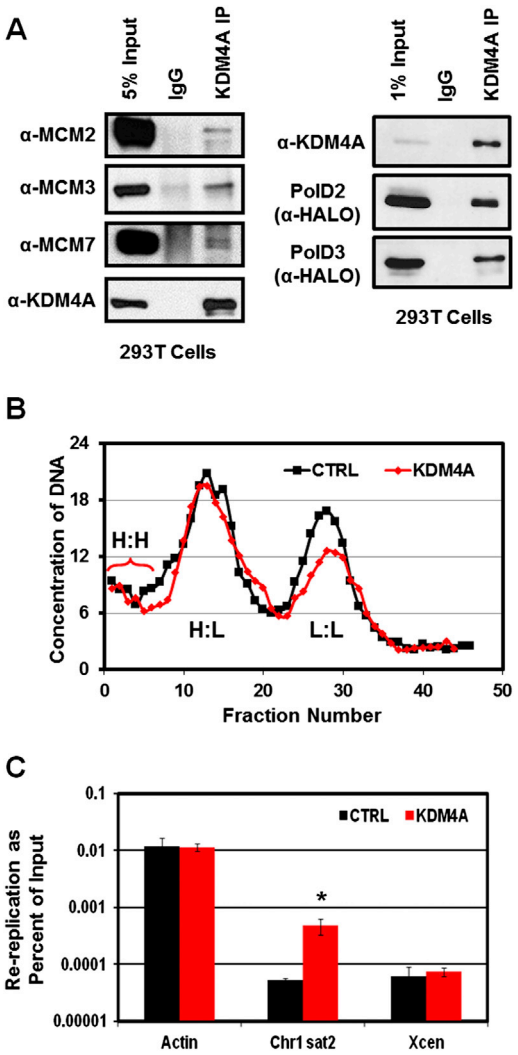

Figure S5. KDM4A Associates with Replication Machinery and Promotes Rereplication of KDM4A Target Regions, Related to Figure 5

(A) Western blots of co-immunoprecipitation of endogenous KDM4A with the indicated licensing and replication machinery in 293T Cells.

(B) A representative CsCl density gradient curve used for determining re-replication of KDM4A target regions. Data are presented as the DNA concentration of the indicated fraction (*x* axis) taken from the bottom of the CsCl gradient. The positions of the light:light (L:L) and heavy:light (H:L) peaks and the heavy:heavy (H:H) region taken for analysis are indicated.

(C) A graph depicting the KDM4A-dependent Chr1 sat2 rereplication plotted as a percent of input DNA loaded onto the CsCl gradient. Error bars represent the SEM. Asterisk indicates $p < 0.05$ compared to GFP-CTRL.

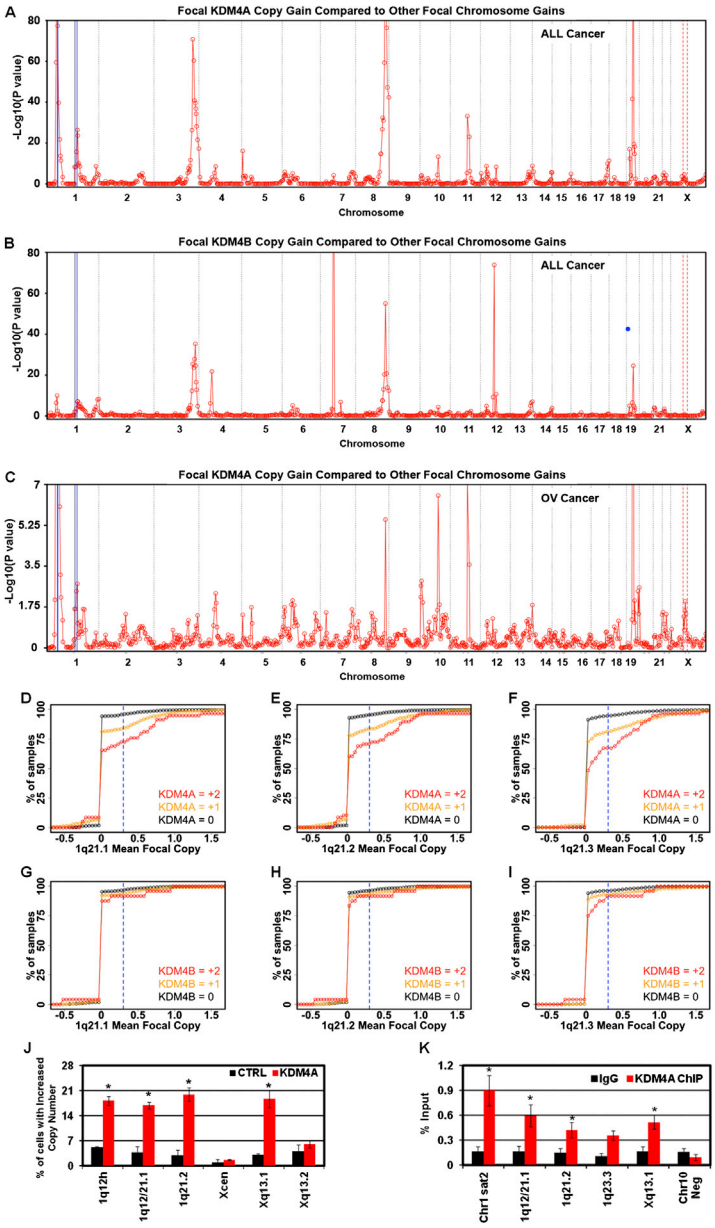

Figure S6. Identification of Cytogenetic Bands Coamplified with KDM4A in Cancer, Related to Figures 6 and 7

(A) Focal amplification of specific cytogenetic bands determined by the statistical test based on the null distribution of mean cytoband copy differences correlated with amplification of *KDM4A* in 4,420 samples across all cancers from the TCGA data set. Graph depicts the –log(10) P-value for correlation of the copy number of each cytogenetic band with the copy number of *KDM4A*. The blue line represents the locus of *KDM4A* (gene-specific significance of $p = 2x10^{-142}$).

(B) Focal amplification of specific cytogenetic bands determined by the statistical test based on the null distribution of mean cytoband copy differences correlated with amplification of *KDM4B* in 4,420 samples across all cancers from the TCGA data set. The blue dot represents the gene-specific significance of *KDM4B*.

(C) Focal amplification of specific cytogenetic bands determined by the statistical test based on the null distribution of mean cytoband copy differences correlated with amplification of *KDM4A* in 547 ovarian cancer samples. The blue line represents the locus of *KDM4A* (gene-specific significance of $p = 1.4x10^{-42}$). For each co-amplification plot, blue shaded regions indicate 1p11.2 through 1q21.3 and red dashed lines indicate Xp11.2 through Xq13.2.

(D–F) Empirical cumulative distribution function (% of samples possessing mean focal copy number less than or equal to the value on the *x* axis) in 1q21.1-1q21.3 with unaltered (0) copy number of *KDM4A*, copy Gain of *KDM4A* (+1), or focally amplified *KDM4A* (+2). The blue dashed lines at 0.3 is a cutoff to define the fraction of co-amplified samples with *KDM4A* amplification in Figure 6D-I.

(G–I) Same as in (D-F) but for *KDM4B*.

(J) KDM4A overexpression increased copy number of 1q12h, 1q12/21.1 and 1q21.2 and Xq13.1 but not X cen or Xq13.2 in 293T cells. Copy number was assessed using the indicated FISH probes.

(K) KDM4A-dependent rereplicated regions are bound by KDM4A. KDM4A ChIP was conducted in 293T cells at regions of re-replication. Error bars represent the SEM. Asterisk indicates $p < 0.05$ compared to CTRL using two-tailed Student's t test.

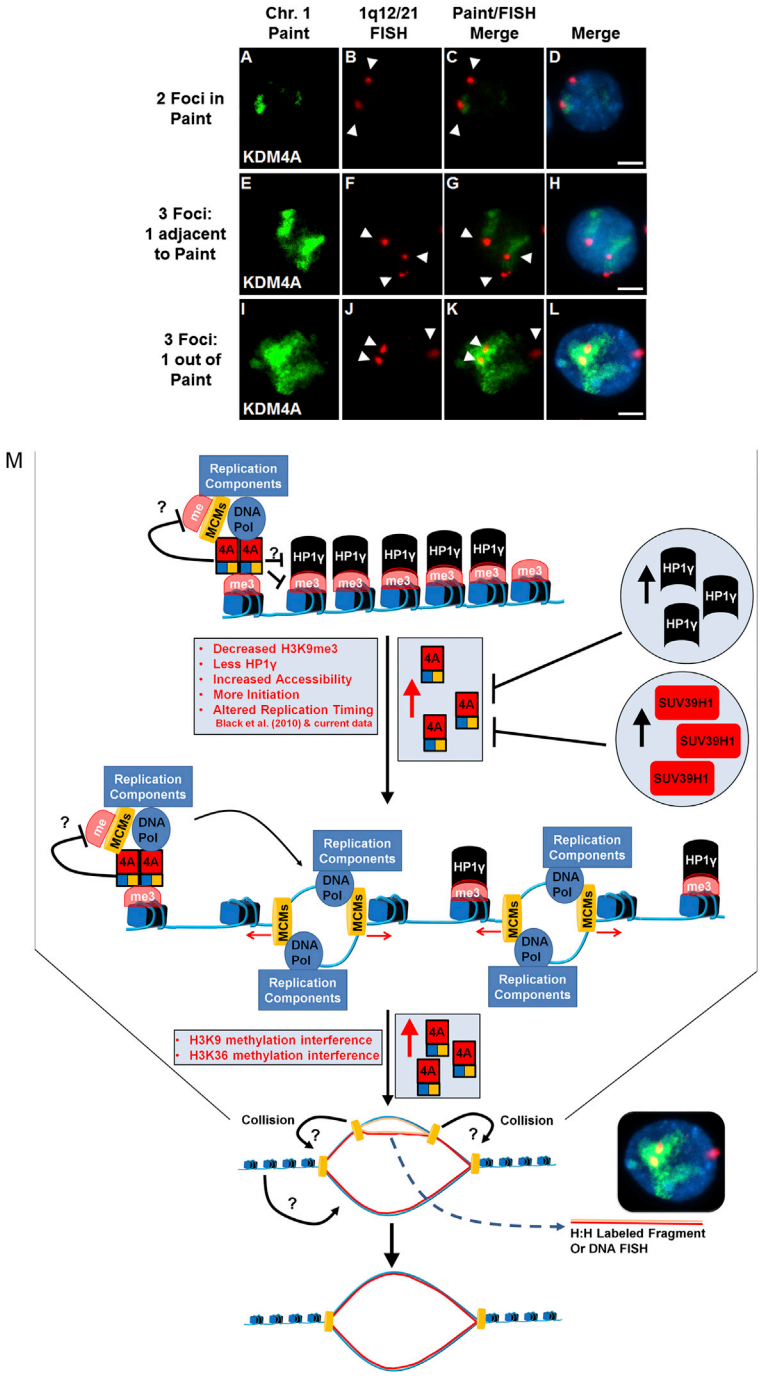

Figure S7. Extra Copies of 1q12/21 Can Be Found Outside of the Chromosome 1 Domain in Interphase Cells, Related to Figure 7

(A–L) Combined Chromosome 1 Paint (Green) and 1q12/21 FISH (Red) demonstrates that extra copies of 1q12/21 can be found adjacent to or outside chromosome 1 domains. Scale bar represents 5 μm.

(M) Schematic depicting the model by which KDM4A could promote copy number gain. Our results support a model where increased expression of KDM4A promotes recruitment of KDM4A to specific genomic regions and promotes rereplication. Increased KDM4A at these loci promotes a more open chromatin environment through removal of H3K9me3 and eviction of HP1γ. Increasing levels of Suv39h1 or HP1γ is sufficient to block this altered chromatin state. These altered chromatin domains could then support rereplication through increased recruitment of MCMs and DNA polymerases, which could be facilitated directly through interactions with KDM4A. Alternatively, the more open chromatin generated by KDM4A could indirectly promote inappropriate recruitment of MCMs and DNA polymerases to unused or reused origins, thus promoting rereplication. The inappropriate rereplication within these regions could then result in head-to-tail collision of one replication fork chasing another. These collisions would then generate extrachromosomal DNA fragments. The "?" represent possibilities that need further testing.